Nucleon Form Factors Measured with BLAST

John Calarco - University of New Hampshire

HUGS – June, 2006

Outline

- **Overview and Motivation**
  - Introduction
  - Existing Methods & Data
  - Phenomenological Fits
  - Theoretical Models
- **Results**
  - Asymmetries
  - $\mu G_E^p/G_M^p$
  - G_M^n
  - G_E^n
- Comparsion to models

Form Factors

- Form Factor definition

$$F(q^2) \equiv \int d^3x\, e^{-iq\cdot x}\rho(x) = 1-\frac{1}{6}\langle r^2\rangle q^2+\mathcal{O}(q^4)$$

- Nucleon current

$$\Gamma^\mu = F_1\gamma^\mu + \frac{i}{2M}F_2 i\sigma^{\mu\nu}q_\nu.$$

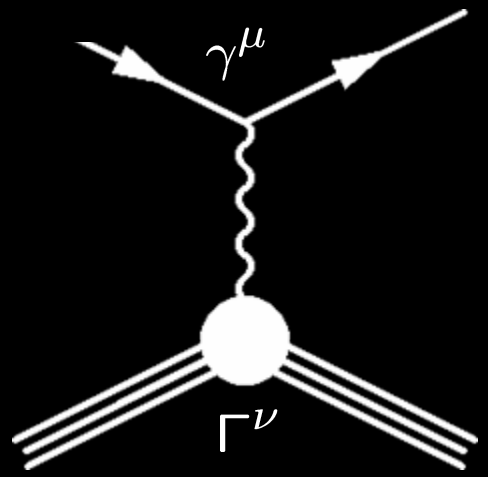

- Fourier Transforms in Breit Frame

$G_E = F_1 - \tau F_2 \longrightarrow$ **1 for p, 0 for n, for $Q^2 \longrightarrow 0$**

$G_M = F_1 + F_2 \longrightarrow$ **2.79 for p, -1.91 for n, for $Q^2 \longrightarrow 0$; $\tau = Q^2/4M^2$**

Existing Methods – Unpolarized X-Section

Rosenbluth Separation:

$$\left(\frac{d\sigma}{d\Omega}\right)^{unpol} = \sigma_{Mott} f_{recoil}^{-1} \left[\frac{G_E^{P\,2} + G_M^{P\,2}}{1+\tau} + 2\tau G_M^{P\,2} \tan^2\left(\theta_e/2\right)\right]$$

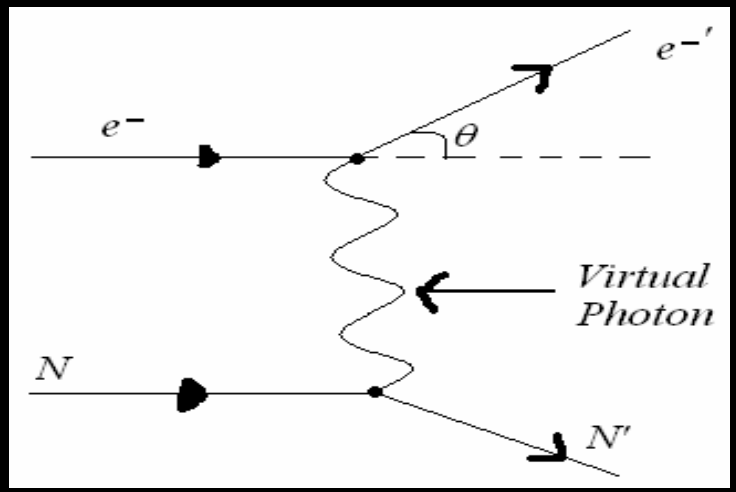

$$\tau = \frac{Q^2}{4M_p^{\,2}}$$

- For $Q^2 > 1$ (GeV/c)^2 the electric form factor is difficult to measure

- At low Q^2, the magnetic form factor becomes difficult to extract

- Mott cross section describes the scattering of a spin ½ electron off a spinless, point-like nucleon:

$$\left(\frac{d\sigma}{d\Omega}\right)_{Mott} = \frac{\alpha^2 \cos^2\left(\frac{\theta}{2}\right)}{4E^2 \sin^4\left(\frac{\theta}{2}\right)\left(1 + 2(E/M_p)\sin^2\left(\frac{\theta}{2}\right)\right)}$$

World Unpolarized Data - G_E^p

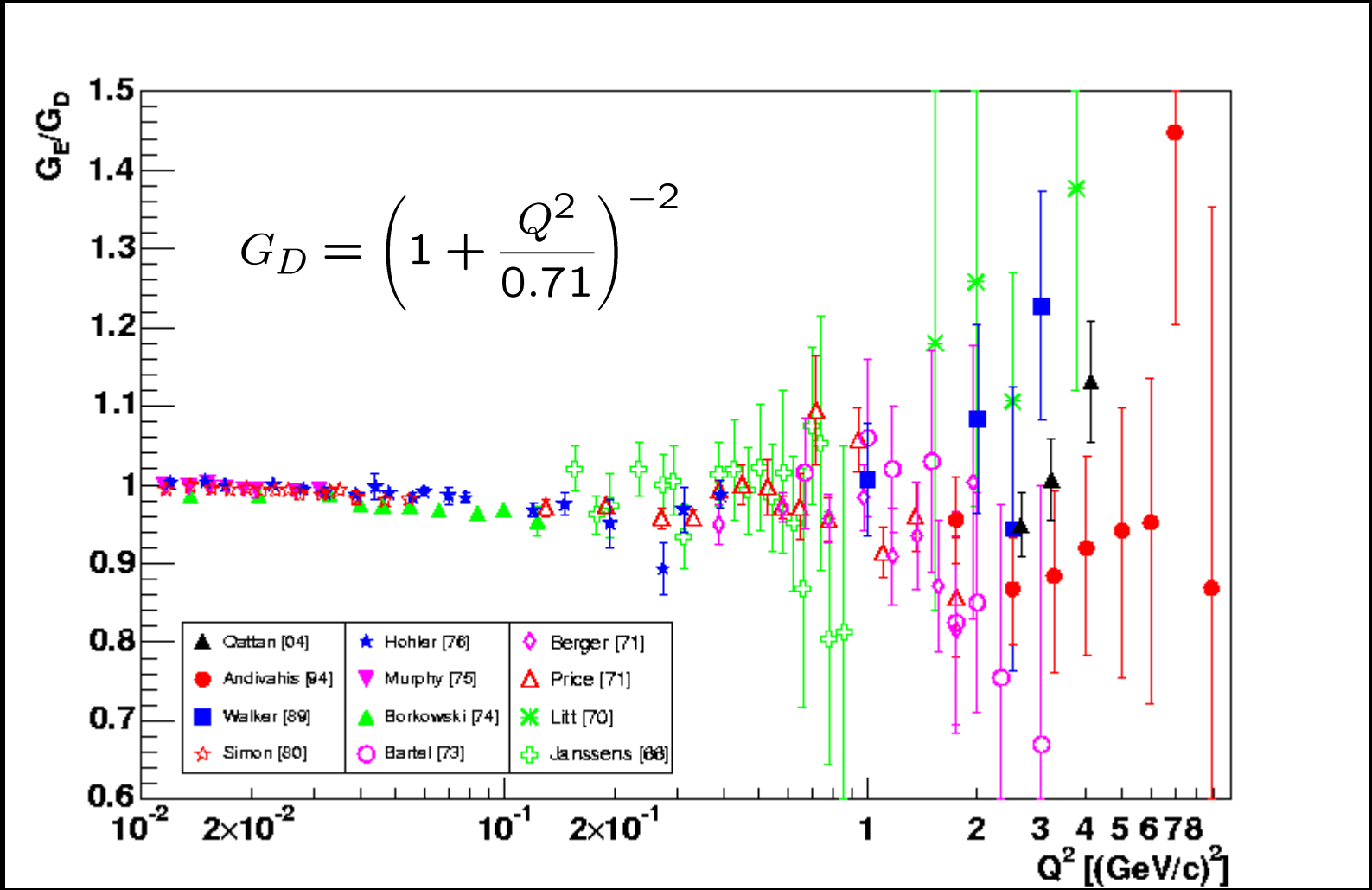

World Unpolarized Data - G_M^p

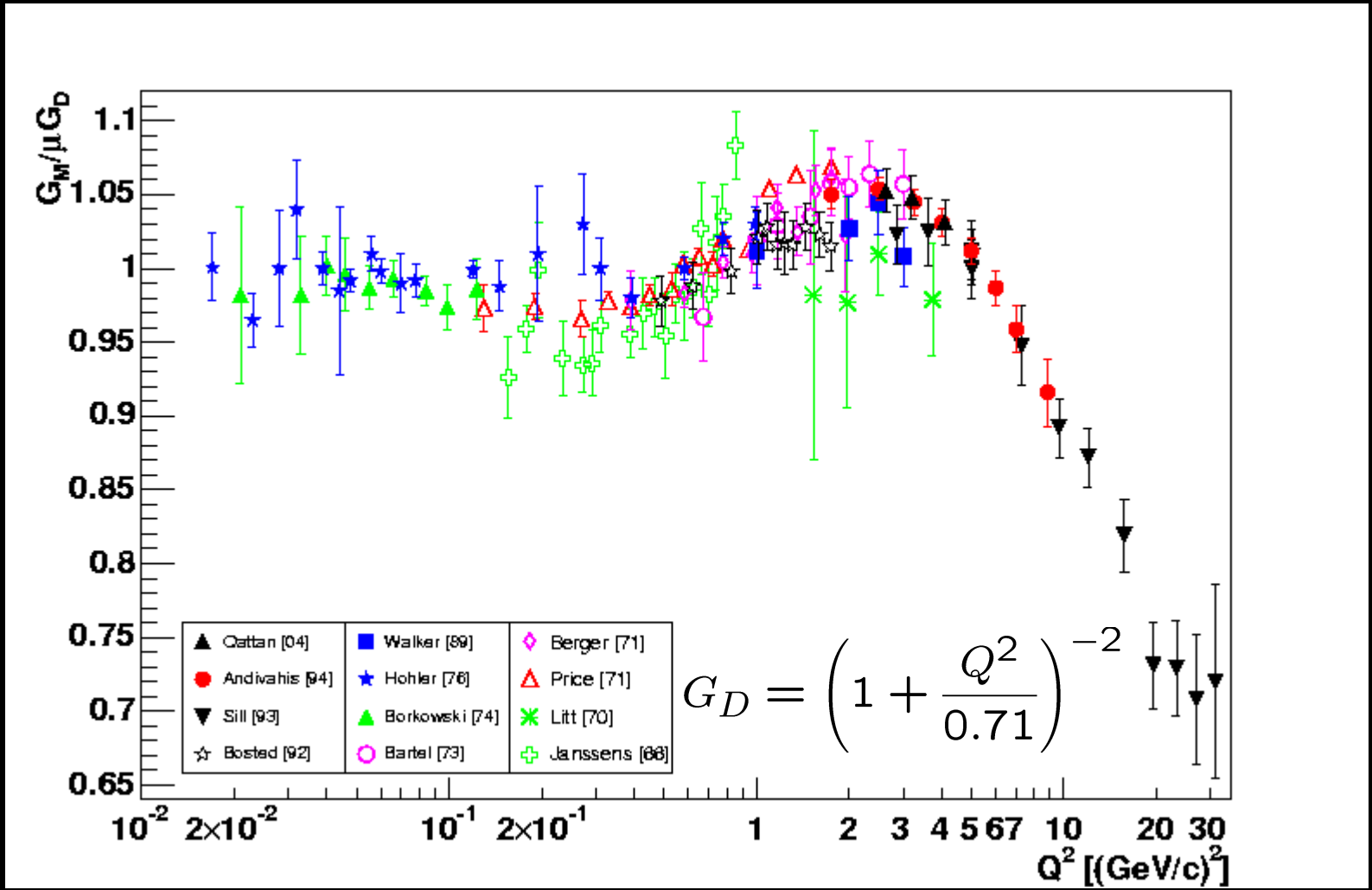

$\mu G_E^p/G_M^p$ – Unpolarized Data

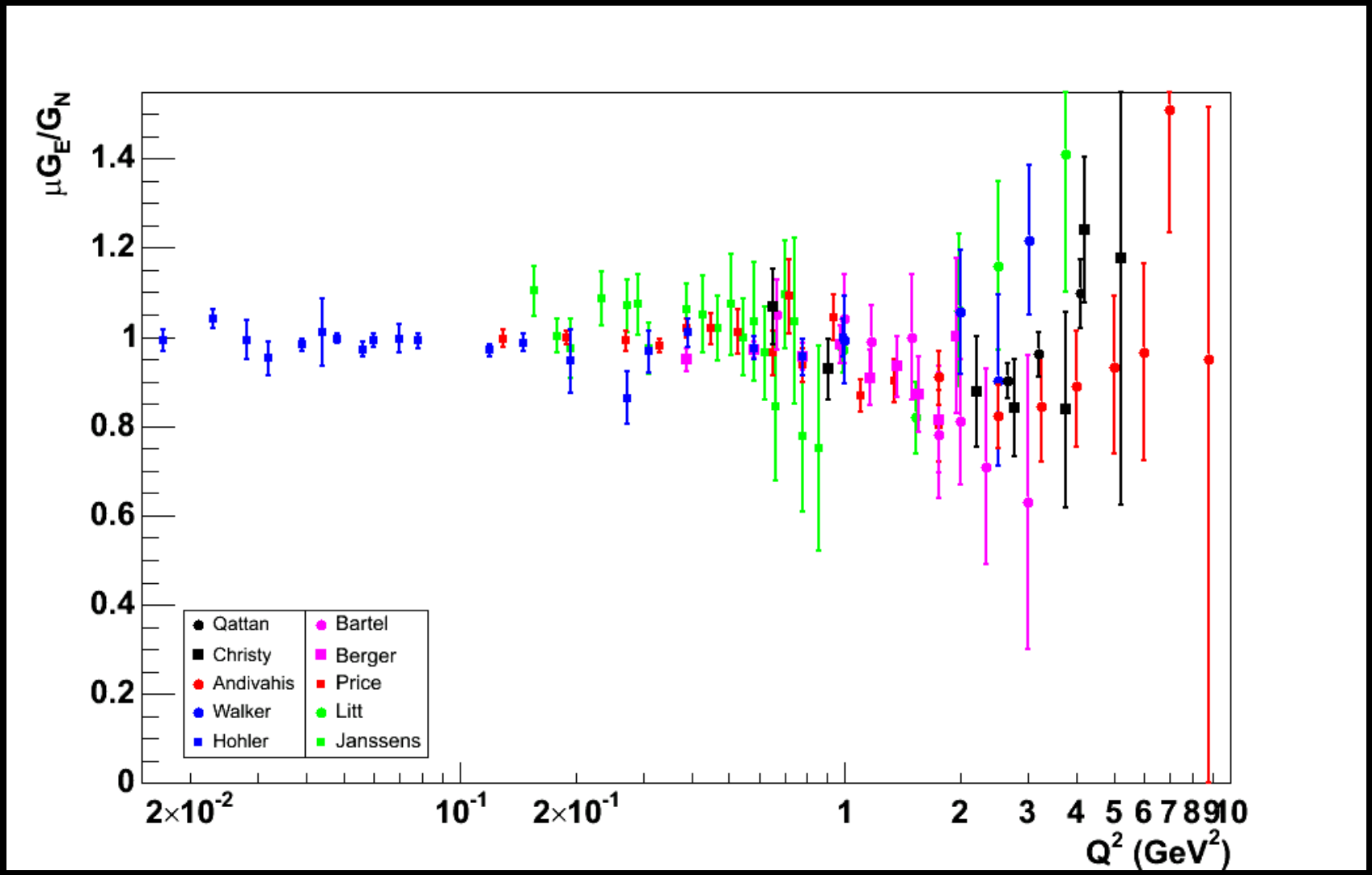

Existing Methods – Polarization Transfer

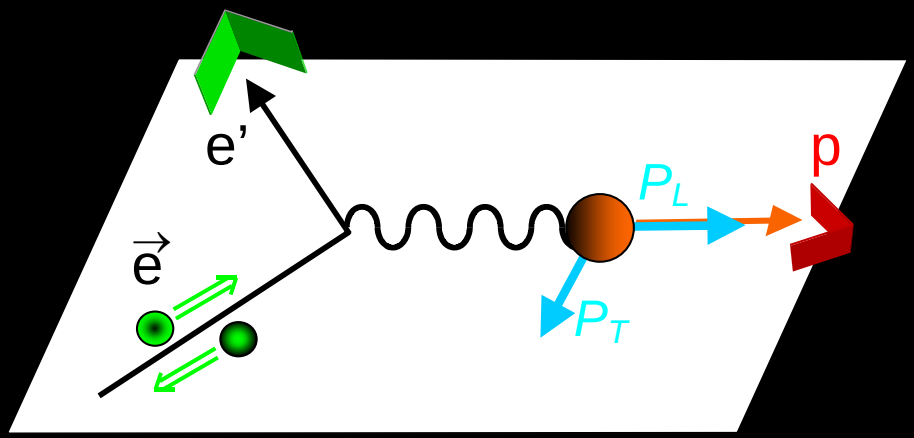

- Polarization transfer measurements use a Focal Plane Polarimeter (FPP)

- P_t and P_l of the scattered proton are measured simultaneously (using ^{12}C)

- G_E^p/G_M^p is measured directly:

$$\frac{G_E^P}{G_M^P} = -\frac{P_t}{P_l}\frac{E+E'}{2M_p}\tan\left(\frac{\theta_e}{2}\right)$$

G_E^p/G_M^p – Polarized Data

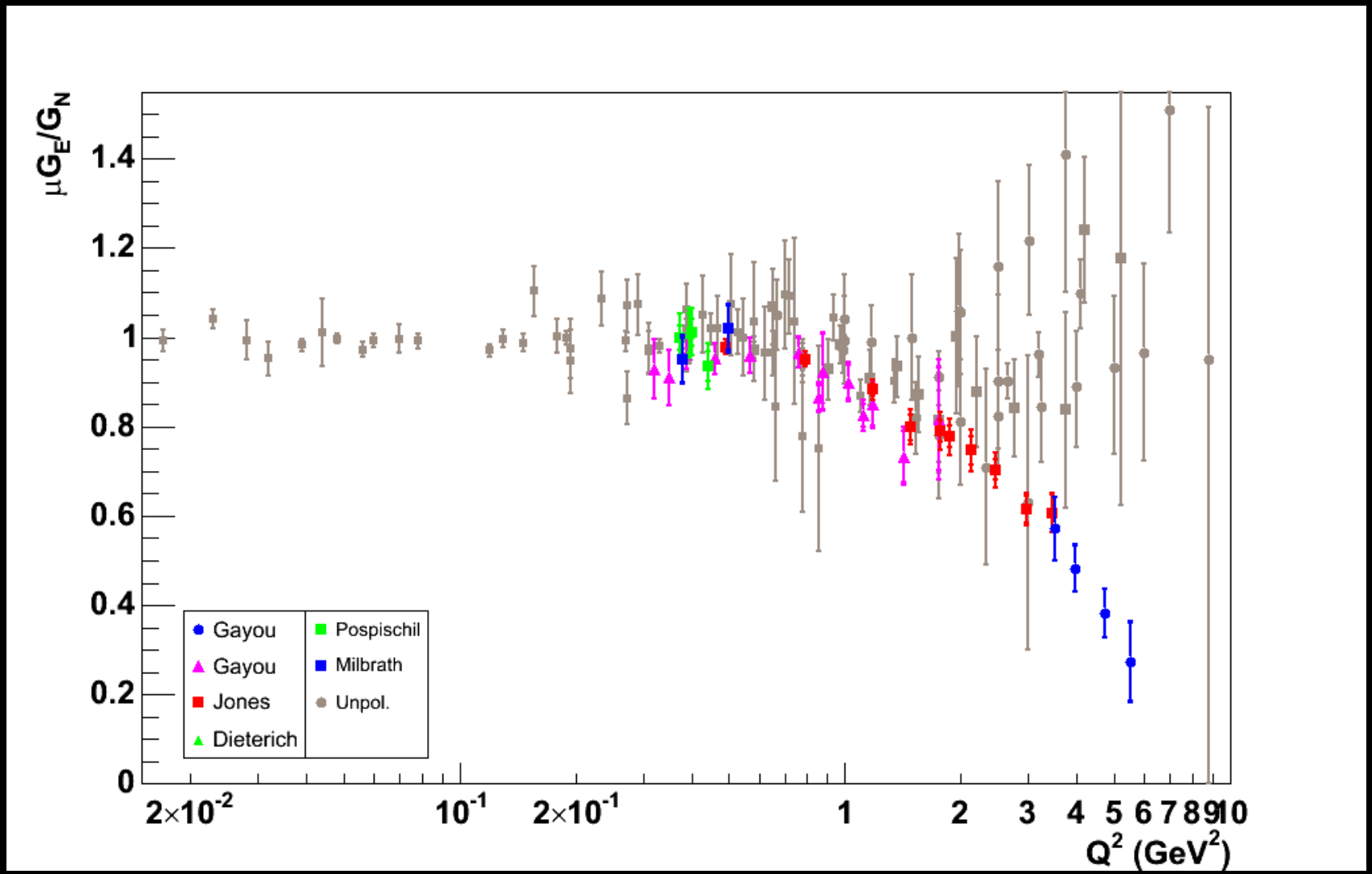

Two-Photon Exchange Contributions

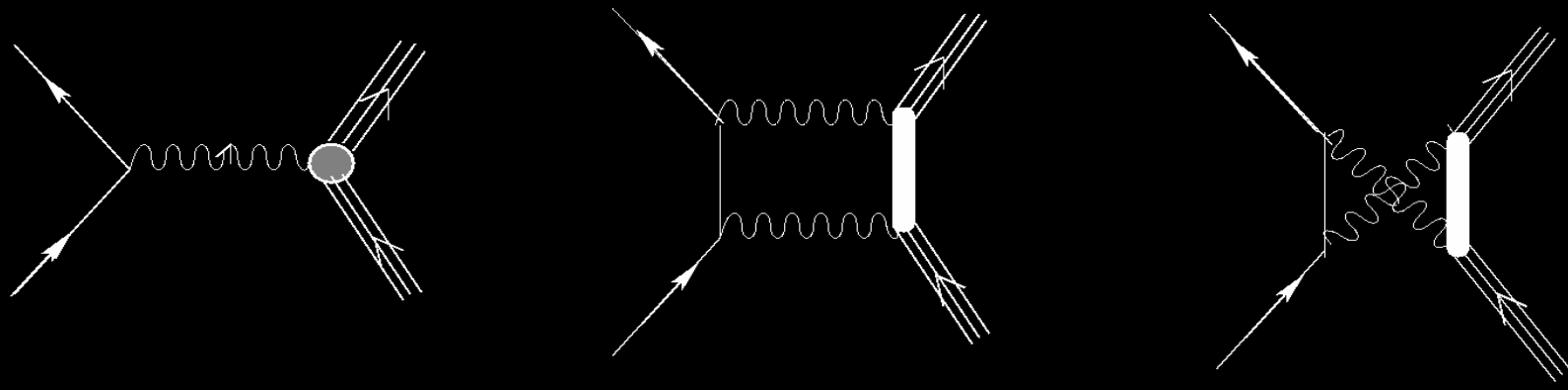

- Guichon and Vanderhaegen (2003): although small (few %) the 2-photon effect is accidentally amplified in the Rosenbluth method!

- Blunden *et al.* (2003) did a first model-dependent calculation of the 2-photon effect and found small corrections with strong angular dependence at fixed Q^2 , proving significant for the Rosenbluth method – they explained about half of the discrepancy!!

- Chen *et al.* (2004) related the 2-photon effect to the GPD and resolved most of the discrepancy between unpolarized and polarized data!!!

Phenomenological Fits

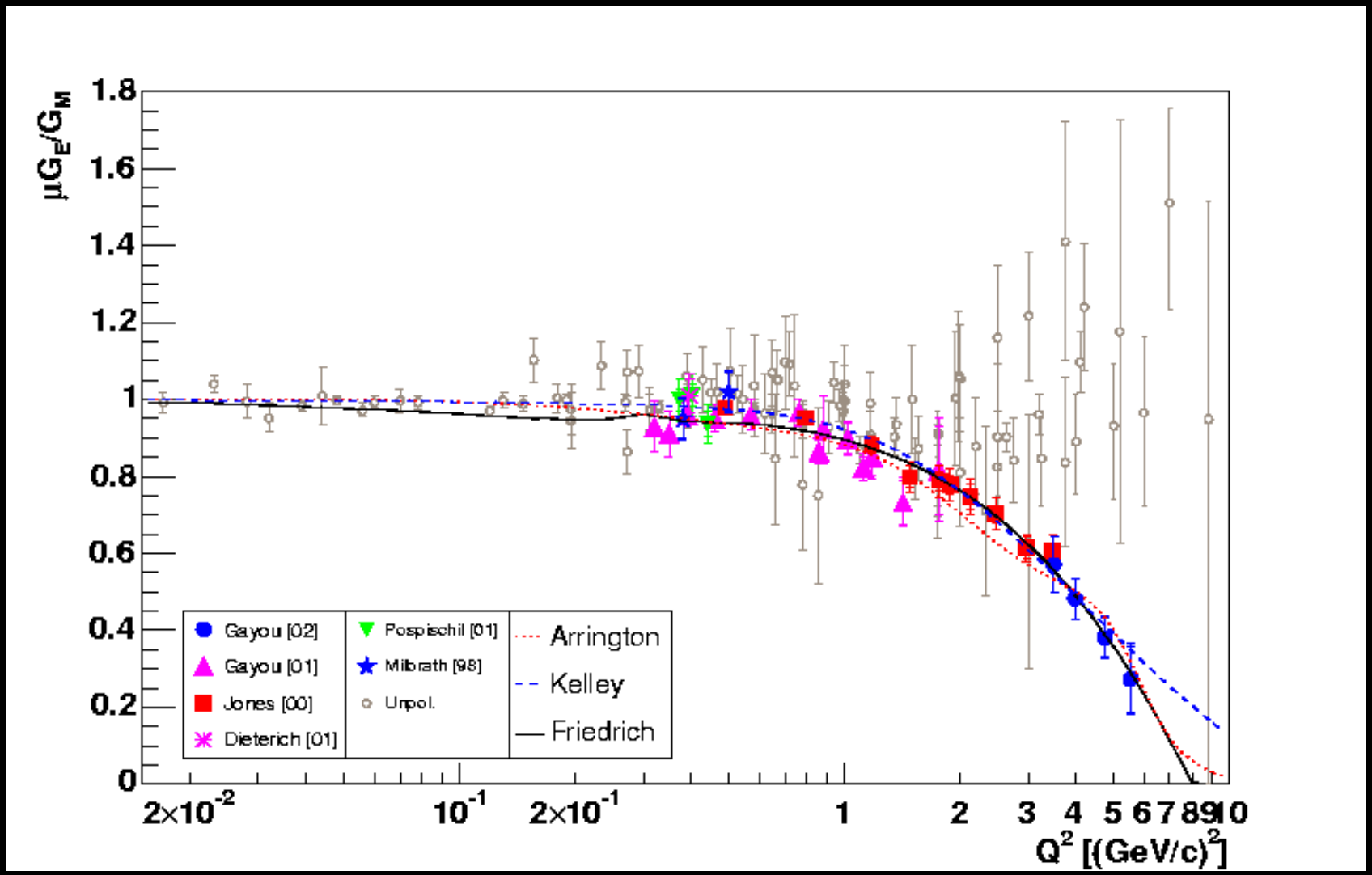

Theoretical Calculations

- Direct QCD calculations

- pQCD scaling at high Q^2
- Lattice QCD at low Q^2

- Meson Degrees of Freedom

- Dispersion analysis, Höhler *et al*. 1976
- Vector Meson Dominance (VMD), Lomon 2002
- Soliton Model, Holzwarth 1996

- QCD based constituent quark models (CQM)

- LF quark-diquark spectator, Ma 2002
- LFCQM + CBM, Miller 2002
- LCCQM, Faessler 2006

Theoretical Models

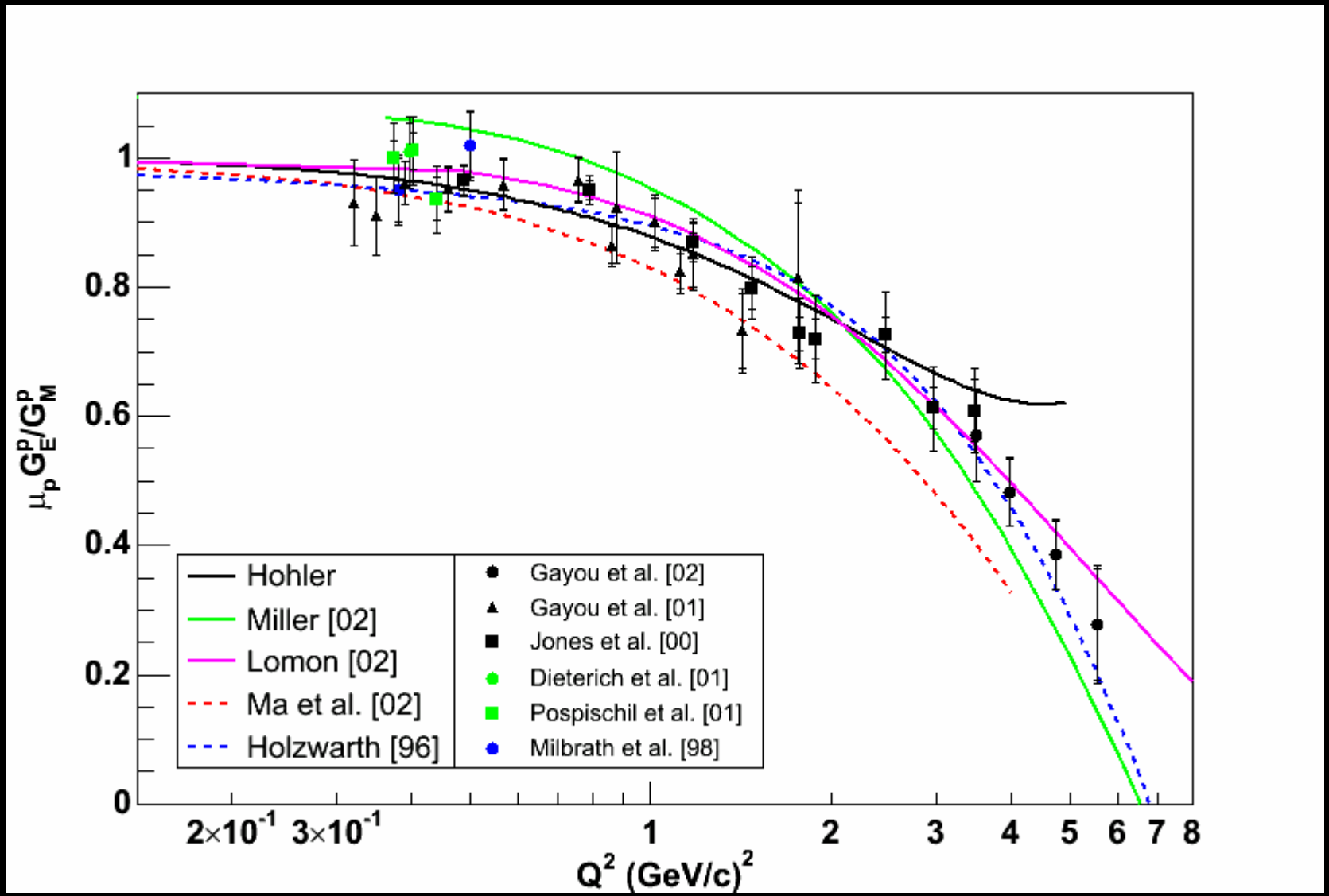

BLAST - Underlying Idea

- Capitalize on the magnetism of the nucleus

- We can polarize a collection of nuclei

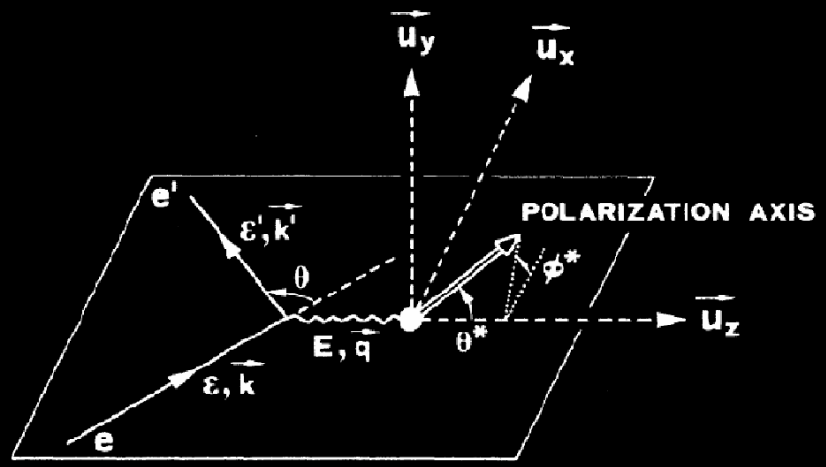

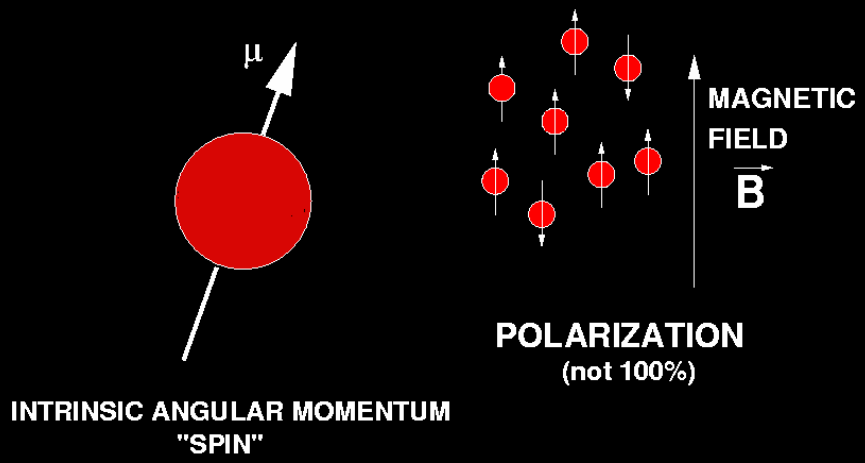

- Polarization observables will manifest themselves!

BLAST - Underlying Idea

- Goal of BLAST was to map G_E^p/G_M^p, G_E^n, G_M^n in the low Q^2 region of the pion cloud
- Systematics different from Polarization Transfer Method
  - insensitive to P_b and P_t
- $Q^2 = 0.1 – 0.9$ (GeV/c) ^{2}
  - input for P.V. experiments
- Exploits unique features of BLAST
  - internal target: pure isotope, fast spin reversal
  - large acceptance: simultaneously measure all Q^2 points
  - symmetric detector: super-ratio measurement

Exploiting BLAST Symmetry

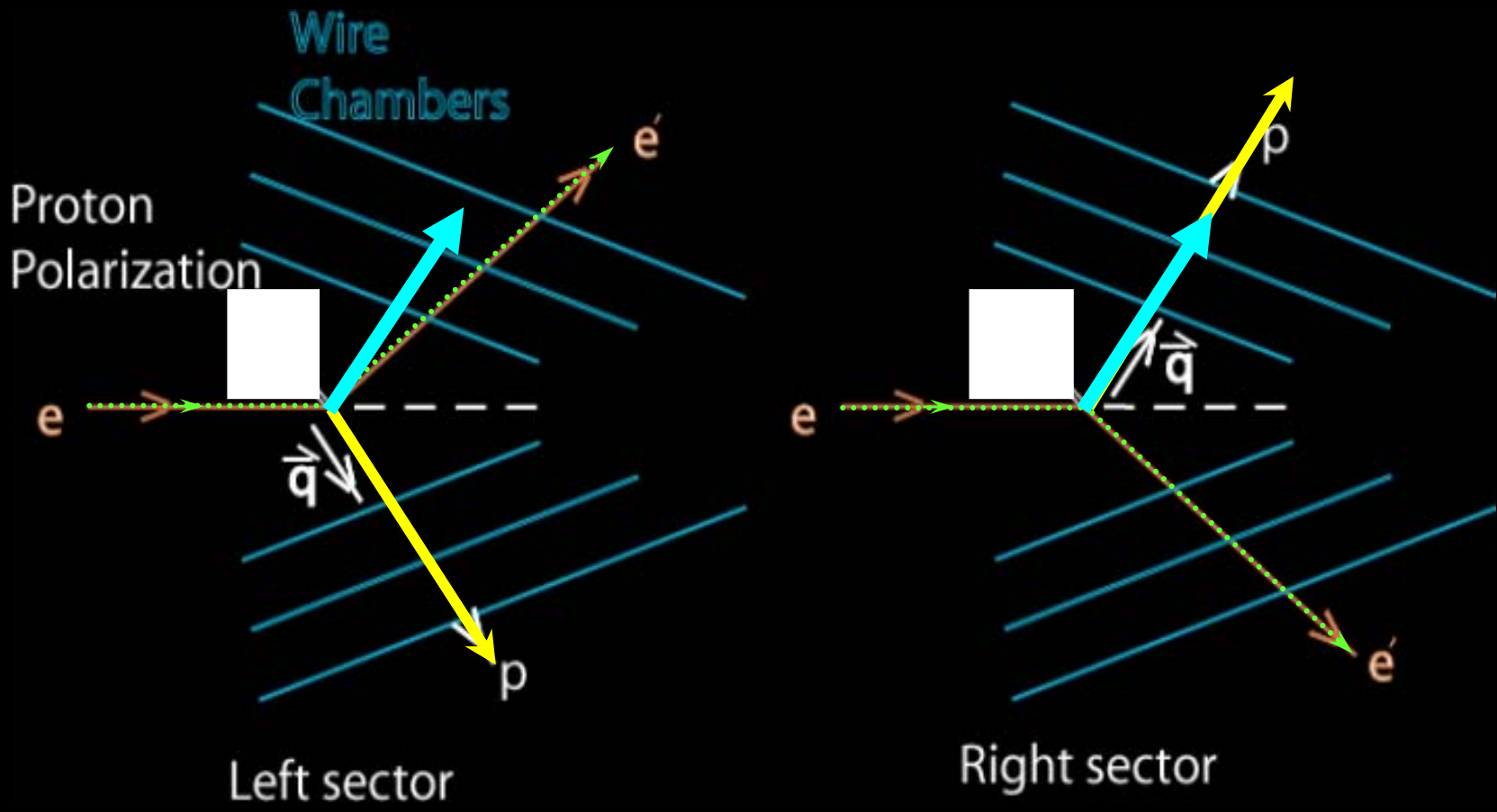

The Super Ratio Technique

- Differential cross section for longitudinally polarized electrons scattered from a polarized proton target:

$$\frac{d\sigma}{d\Omega} = \Sigma + h\Delta$$

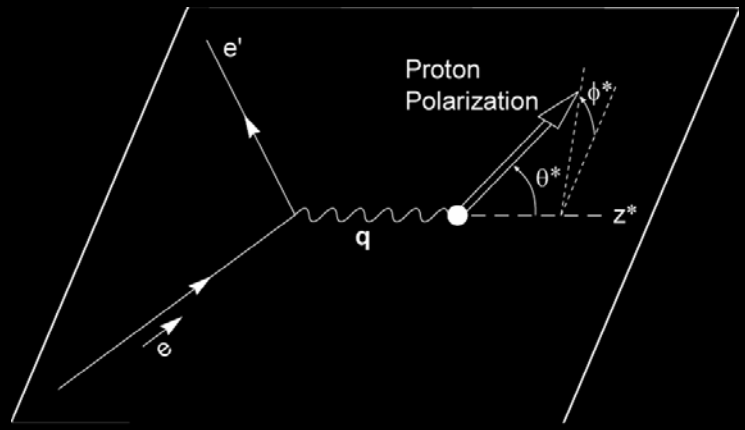

- Spin-Dependent Asymmetry:

$$A \equiv \frac{\Delta}{\Sigma} = -\frac{2\nu_{T'}\cos\theta^* G_M^{P\,2} - 2\sqrt{2\tau(1+\tau)}\nu_{TL'}\sin\theta^*\cos\phi^* G_M^P G_E^P}{(1+\tau)\nu_L G_E^{P\,2} + 2\tau\nu_T G_M^{P\,2}}$$

- Experimental Spin-Dependent Asymmetry:

$$A_{exp} = P_b P_t A = \frac{N_{++} - N_{+-} - N_{-+} + N_{--}}{N_{++} + N_{+-} + N_{-+} + N_{--}}$$

- Super Ratio:

$$R_{exp} \equiv \frac{A_L}{A_R} = \frac{2\nu_{T'}\cos\theta_L^* - 2\sqrt{2\tau(1+\tau)}\nu_{TL'}\sin\theta_L^*\cos\phi_L^* G_E^P/G_M^P}{2\nu_{T'}\cos\theta_R^* - 2\sqrt{2\tau(1+\tau)}\nu_{TL'}\sin\theta_R^*\cos\phi_R^* G_E^P/G_M^P}$$

- Beam and target polarizations cancel out in the super ratio !

Event Selection

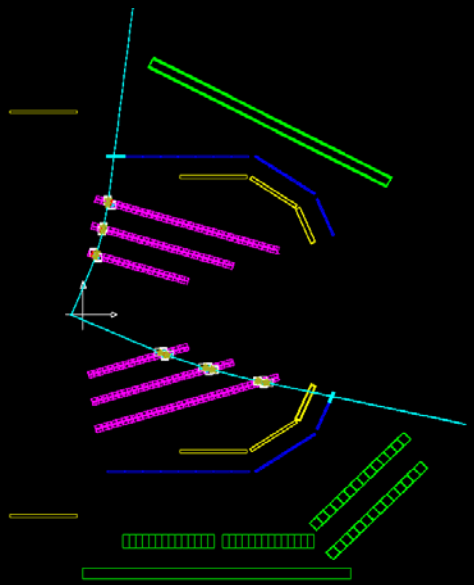

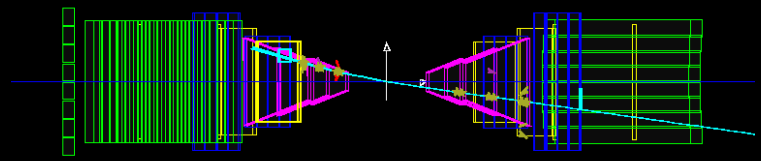

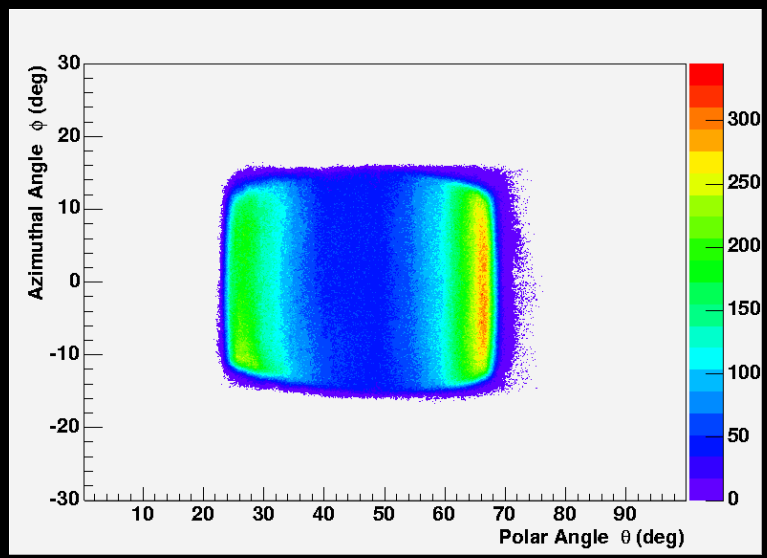

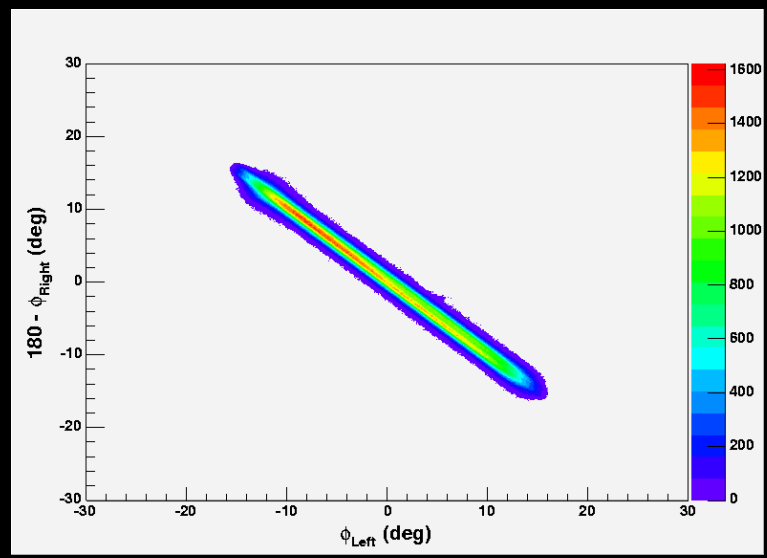

Data Quality

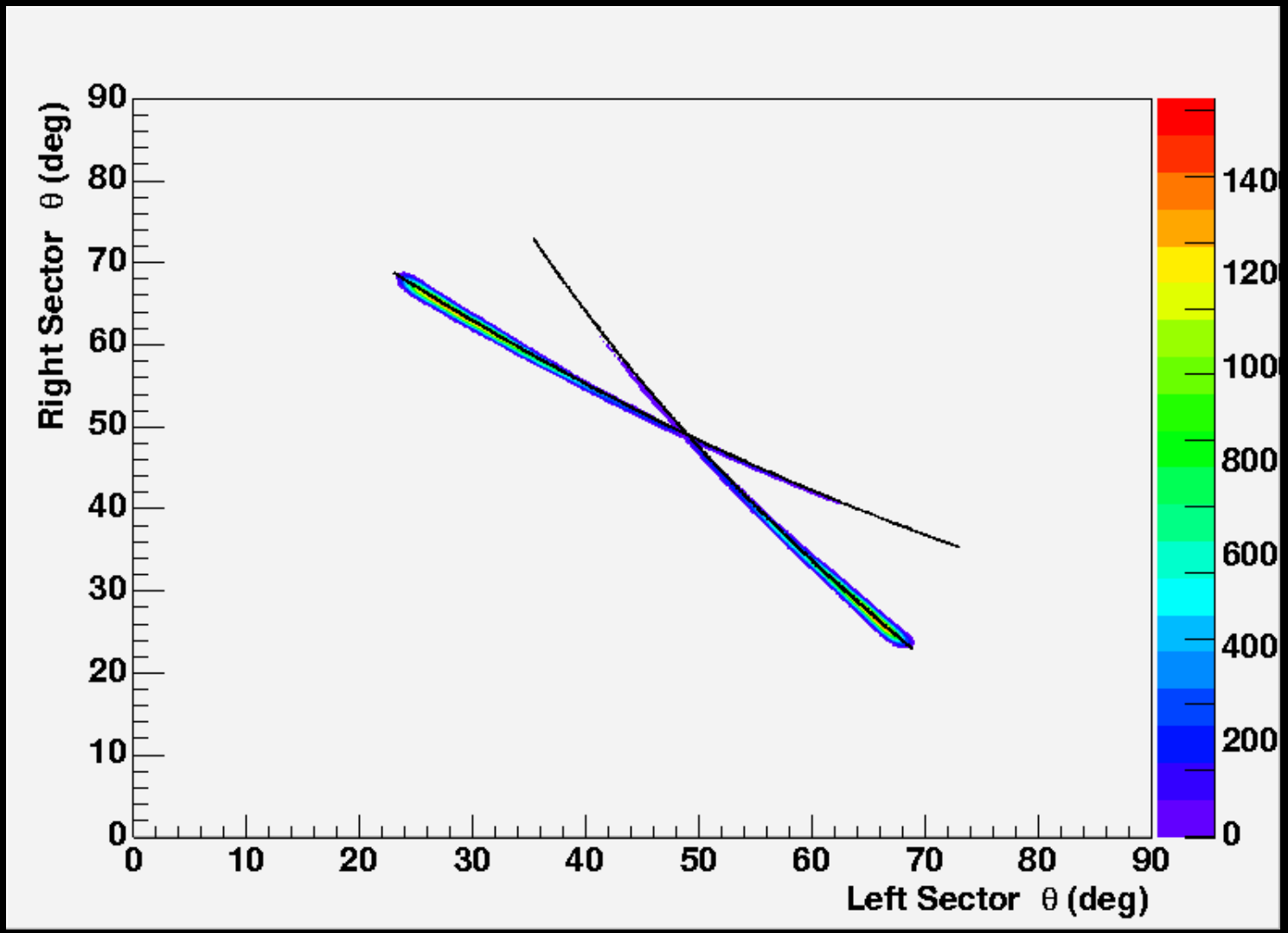

Results - Asymmetries

$$A_{exp} = P_b P_t A = \frac{N_{++} - N_{+-} - N_{-+} + N_{--}}{N_{++} + N_{+-} + N_{-+} + N_{--}}$$

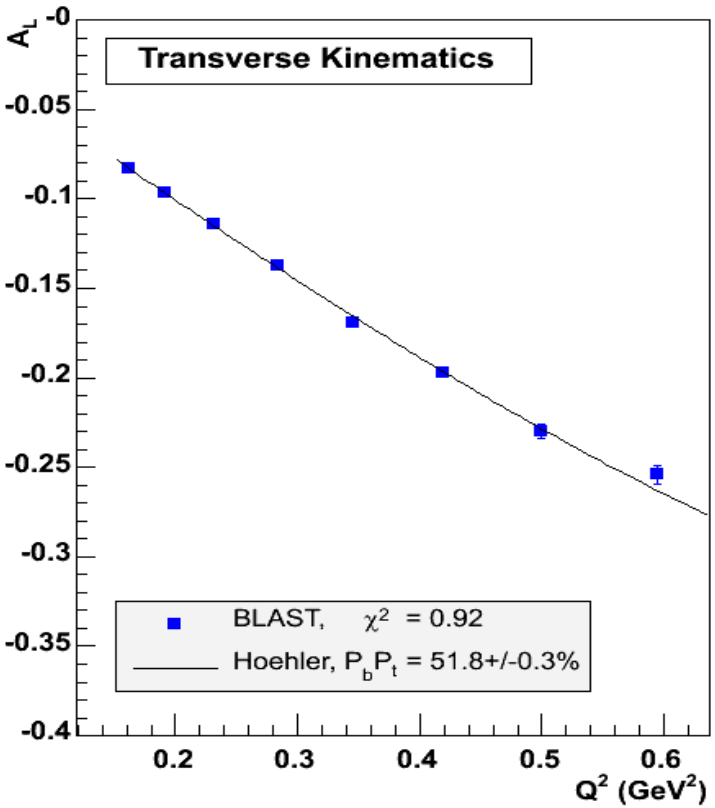

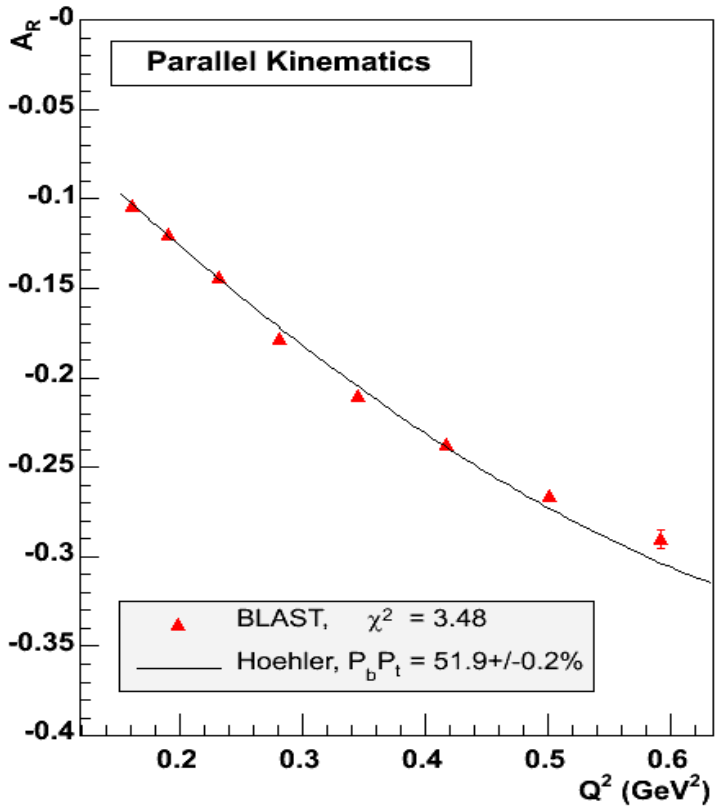

BLAST Left Sector **BLAST Right Sector**

$$A_{ij}(\beta) = P\frac{z_{ij}(\beta) + x_{ij}(\beta)\,R_j}{\epsilon_j\,R_j^2 + \tau_j}$$

i = left,right sector
j = Q^2 bin (1..n)
β = spin angle

- **Single-asymmetry Method**

measure ***P*** first,
use to calculate ***R***

model-dependent

- **Super-ratio Method**

2 equations in ***P***, ***R***

– in each Q^2 bin ***j***
independent measure of polarization in each bin!
2*n* parameters P_j, R_j

- **Global Fit Method**

fit for ***P***, R_1, R_2, …
from all A_{ij} together

model independent
better statistics
***n*+1** parameters
can also fit for β

Extractions of μ G_E/G_M

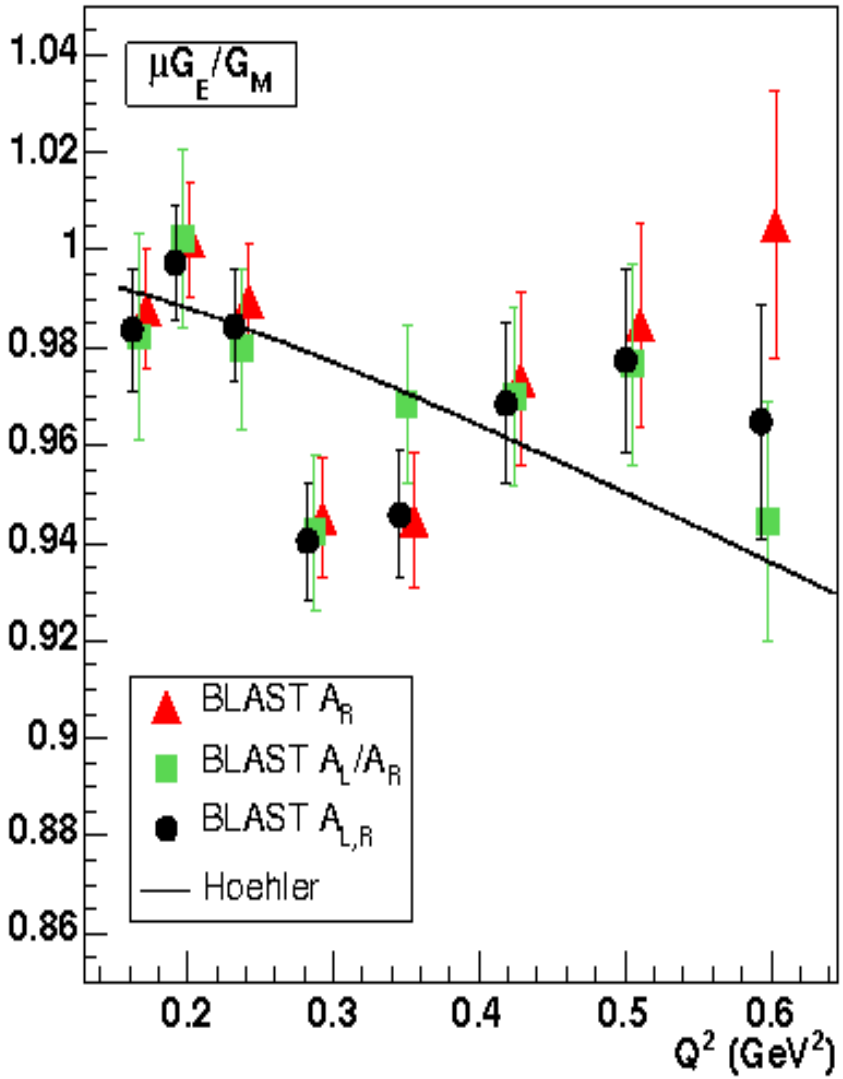

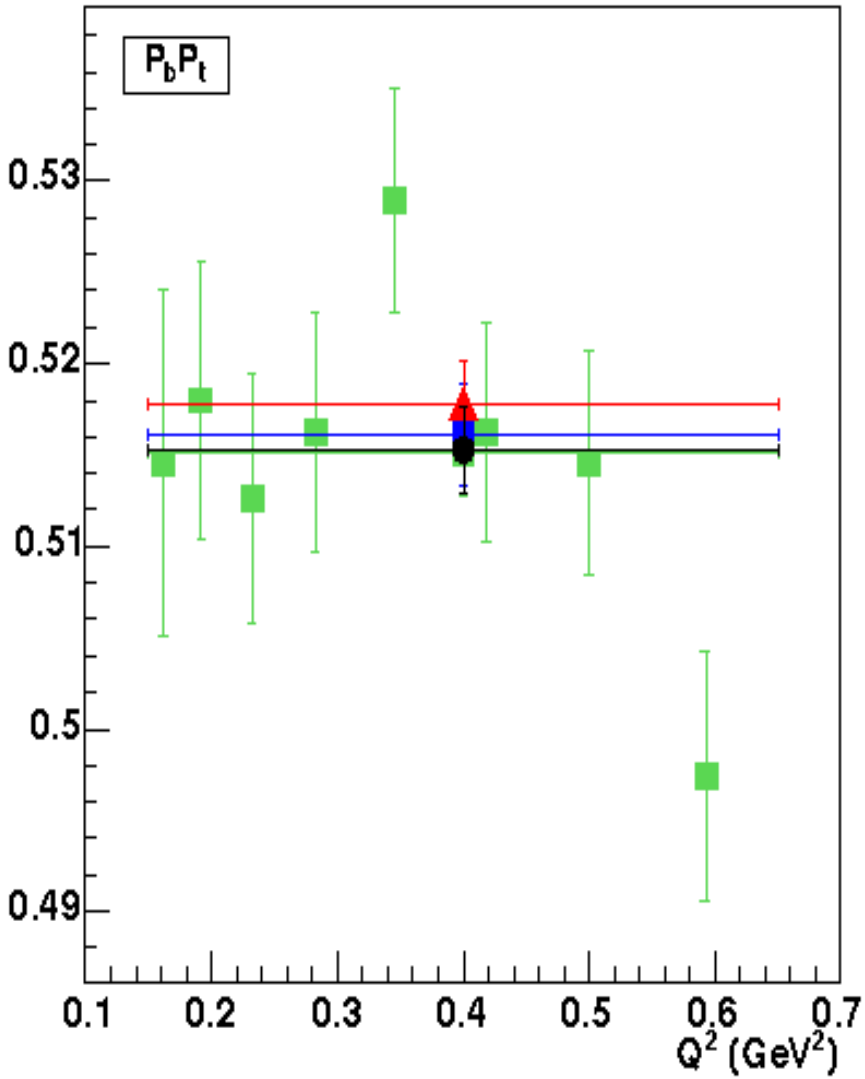

$\mu G_E^p/G_M^p$ Results

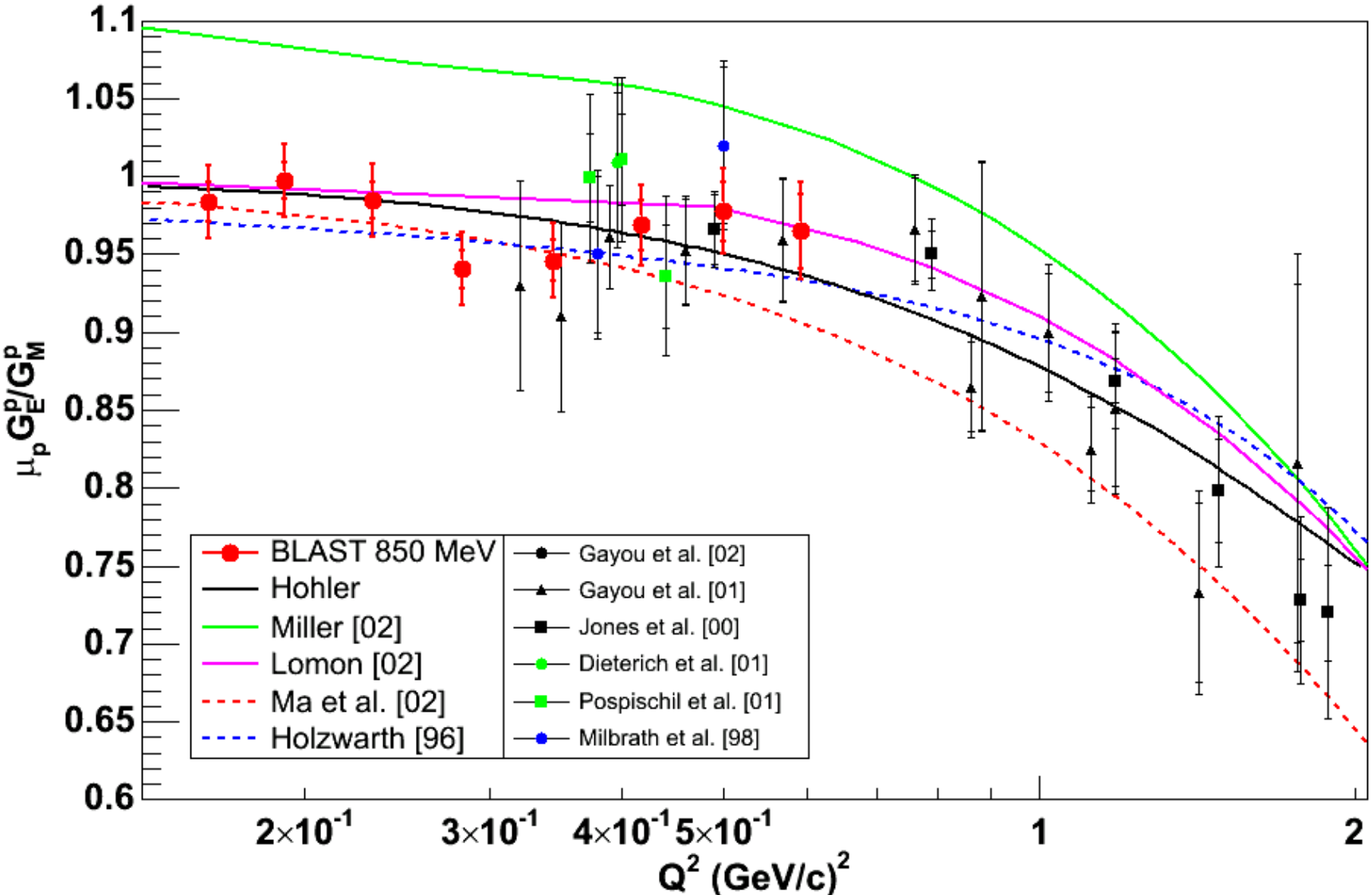

Phenomenological Fit to the Results

- BLAST collaboration fit Friedrich-Walcher parameterization

$$G_E^n = \frac{a_{10}}{(1+Q^2/a_{11})^2} + \frac{a_{20}}{(1+Q^2/a_{21})^2} + a_b Q^2 \left(e^{-\frac{1}{2}\left(\frac{Q-Q_b}{\sigma_b}\right)^2} + e^{-\frac{1}{2}\left(\frac{Q+Q_b}{\sigma_b}\right)^2} \right)$$

- The slope at $Q^2=0$ is an important constraint

$$-\frac{1}{6}\langle r_n^2 \rangle = \frac{dG_E^n}{dQ^2}\Big|_{Q^2=0} = -2\left(\frac{a_{10}}{a_{11}} + \frac{a_{20}}{a_{21}}\right) + 2a_b e^{-\frac{Q_b^2}{2\sigma_b^2}}$$

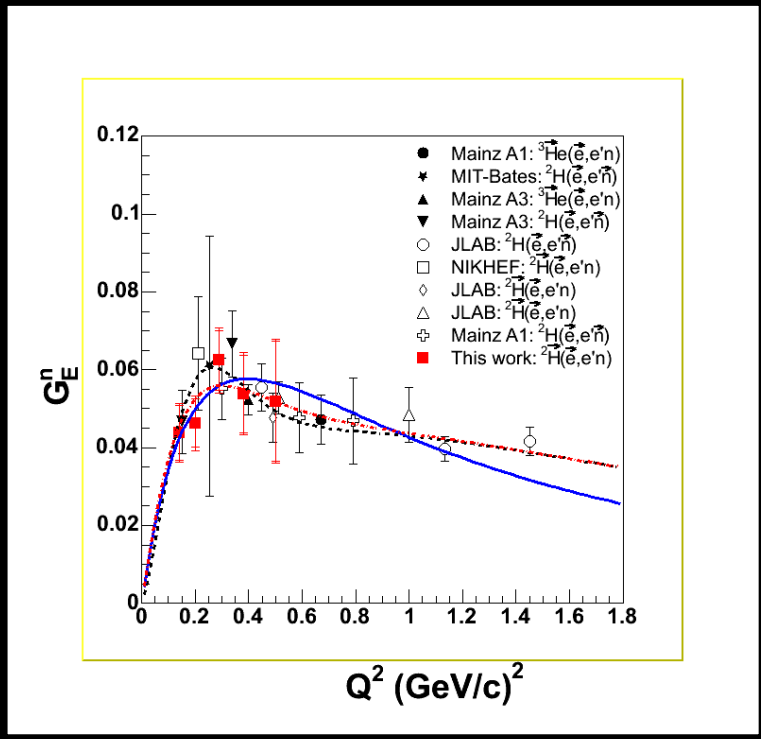

- BLAST data at lowest Q^2 is in good agreement with slope

Nucleon Form Factors in terms of a Pion Cloud and Constituent Quarks

J. Freidrich and Th. Walcher, 2003

- Parametrize the nucleon form factors by

$$G_N(Q^2) = G_s(Q^2) + a_b \cdot Q^2 G_b(Q^2)$$

- a_b is the amplitude of the bump

For example

$$G_E^n = \frac{a_{10}}{(1+Q^2/a_{11})^2} + \frac{a_{20}}{(1+Q^2/a_{21})^2} + a_b Q^2 \left(e^{-\frac{1}{2}\left(\frac{Q-Q_b}{\sigma_b}\right)^2} + e^{-\frac{1}{2}\left(\frac{Q+Q_b}{\sigma_b}\right)^2} \right)$$

Pion Cloud

- Pion as a pair of quarks

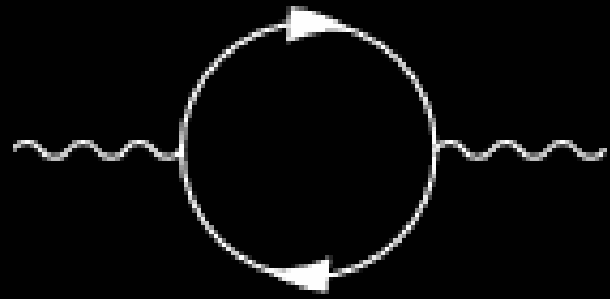

- Just like particles appear in vacuum…

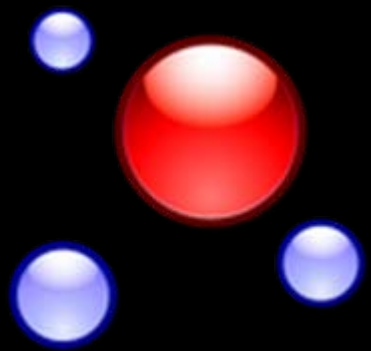

… pions pop up continuously at the nucleon surface

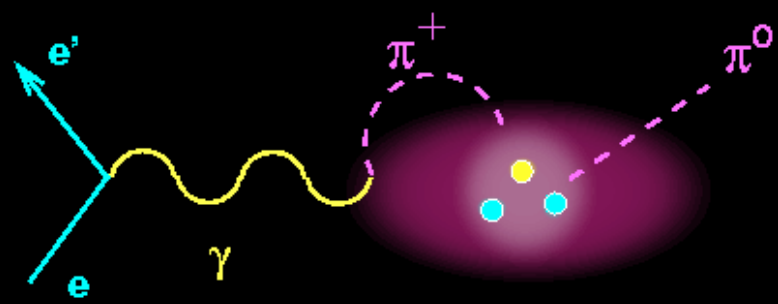

- Pion contribution can be revealed in e-N scattering

The Pion Cloud

- Friedrich – Walcher analysis
- "n" = $an + b(p + \pi^-)$ $\quad a + b = 1$
  $= n + b(p - n + \pi^-)$ ← pol.
- "p" = $ap + b(n + \pi^+)$ $\quad a + b = 1$
  $= p + b(n - p + \pi^+)$ ← pol.
- Pol. → pion cloud
- Effect of pol. on p small since p has net charge $+e$
- Effect of pol. on n large since n has net charge $0e$

World's data on G_E^p

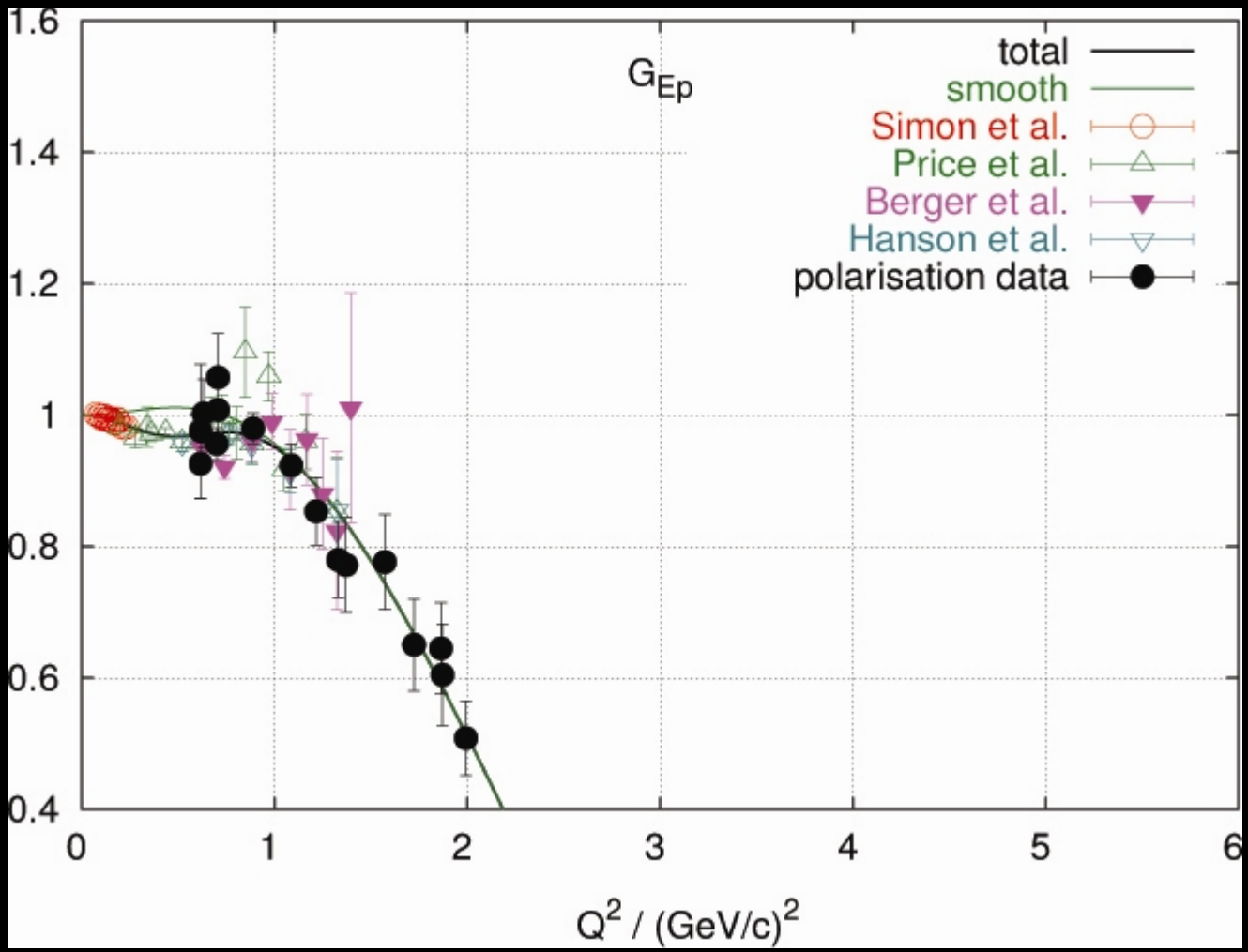

World's data on G_M^p

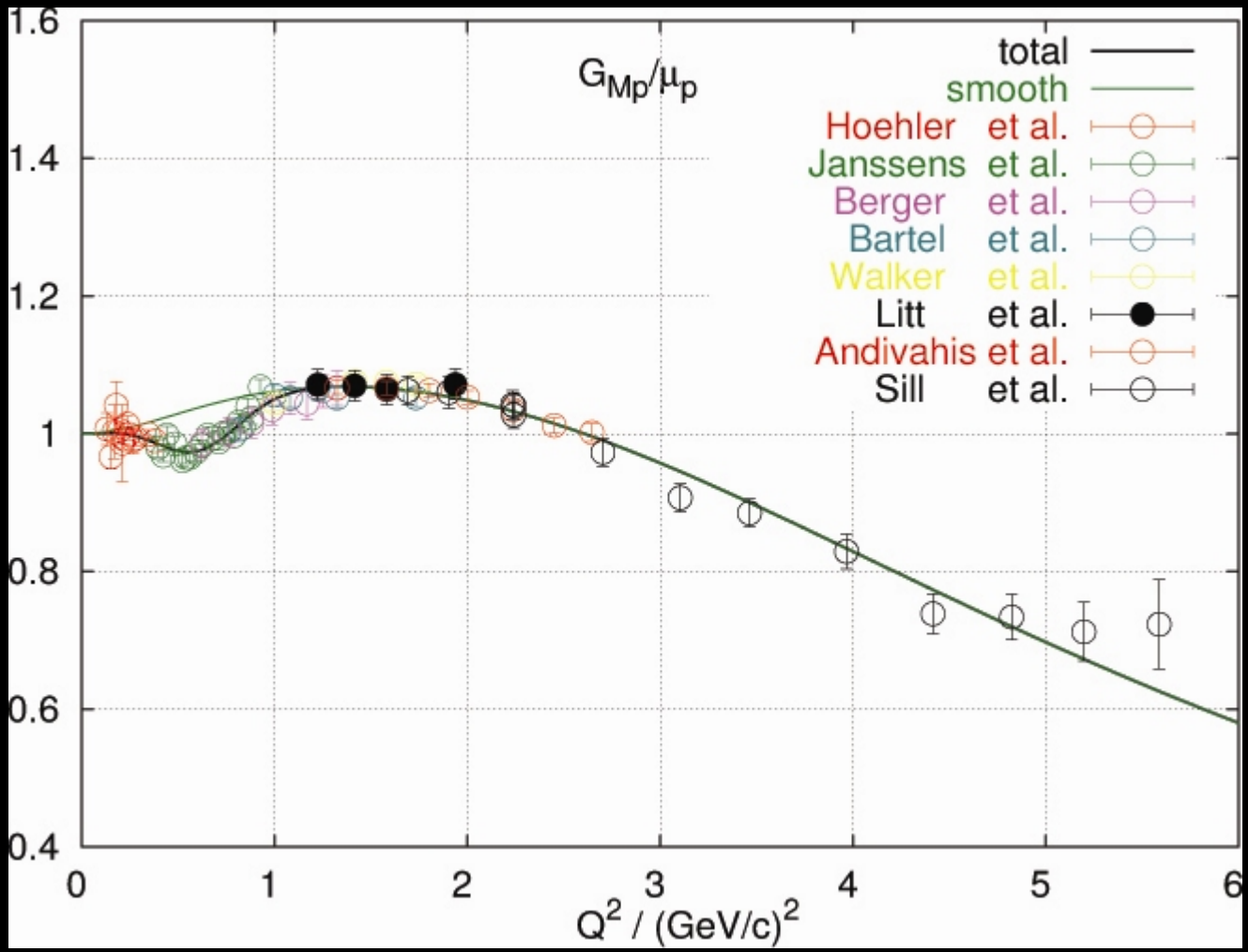

Friedrich-Walcher fit

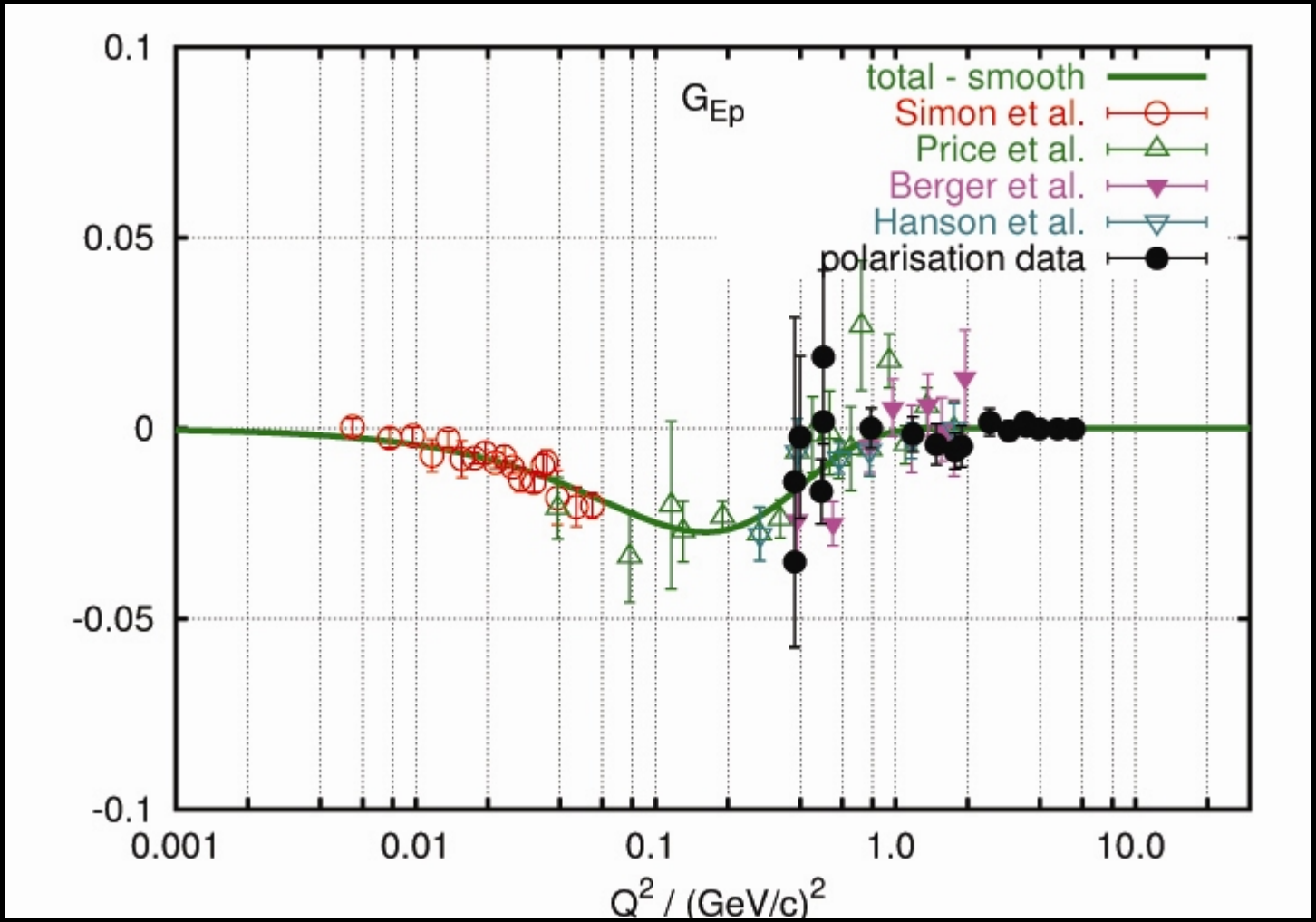

Difference between measured FF and the smooth part

Friedrich-Walcher fit

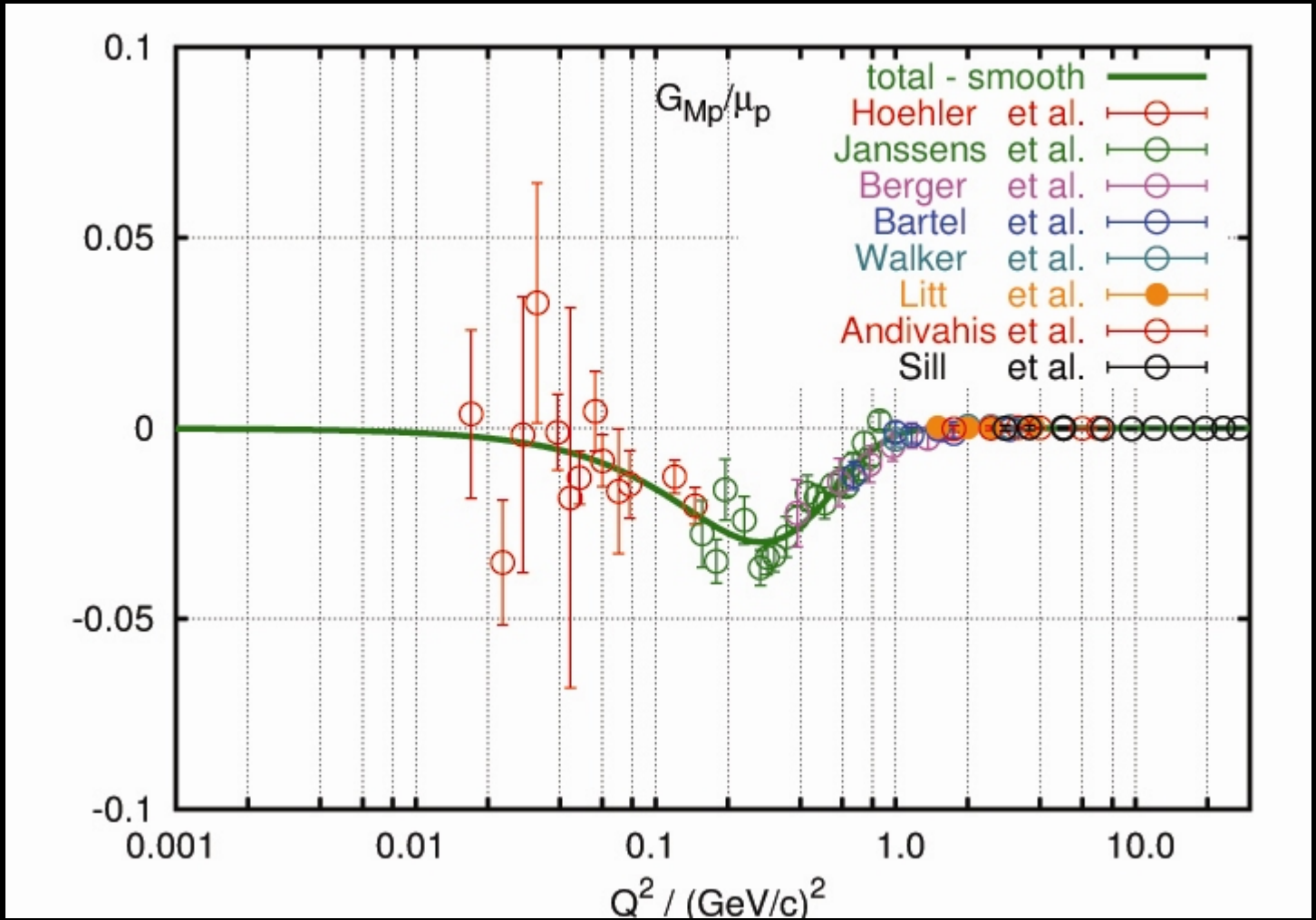

Friedrich-Walcher fit

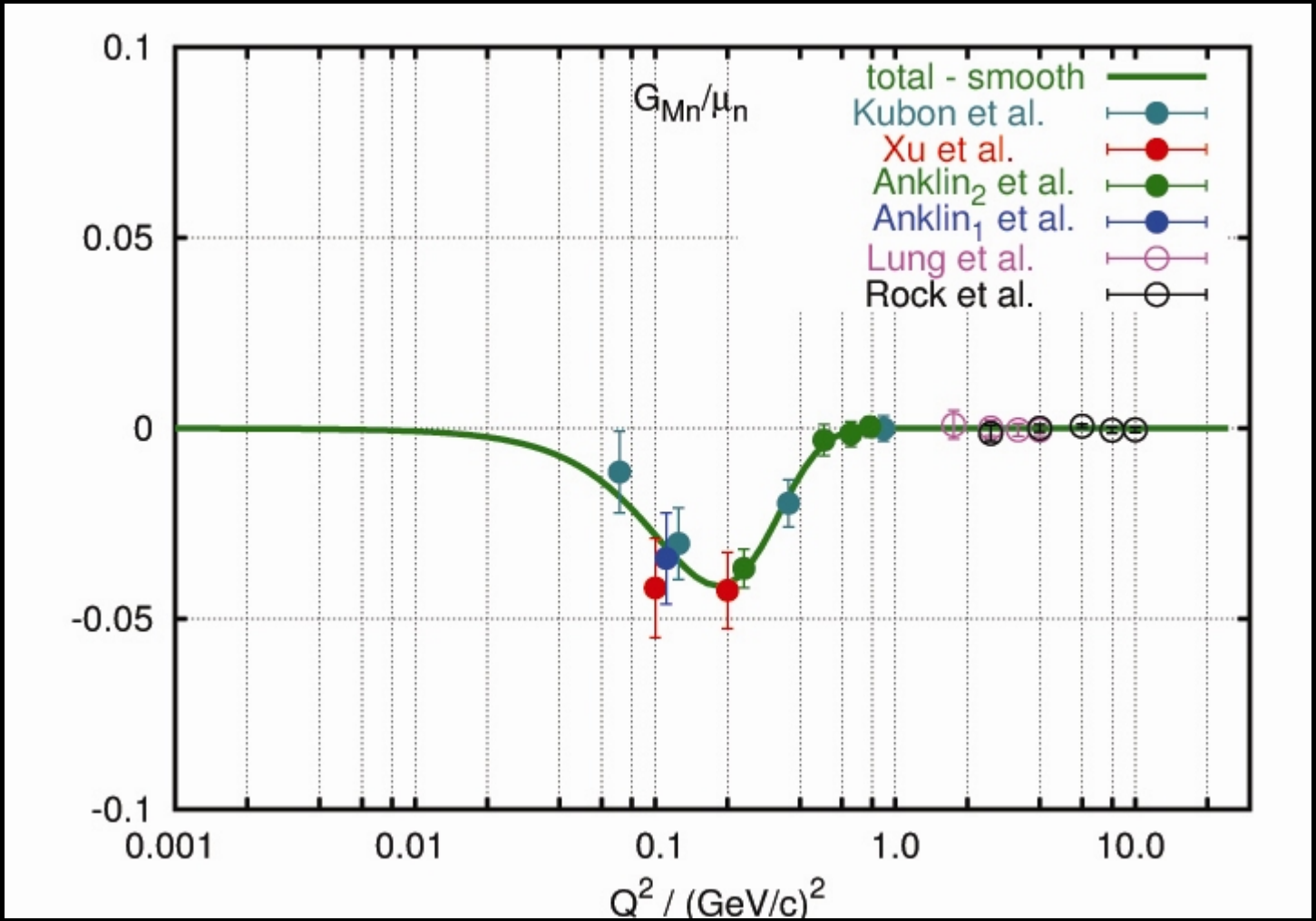

Preliminary BLAST G_e^p data

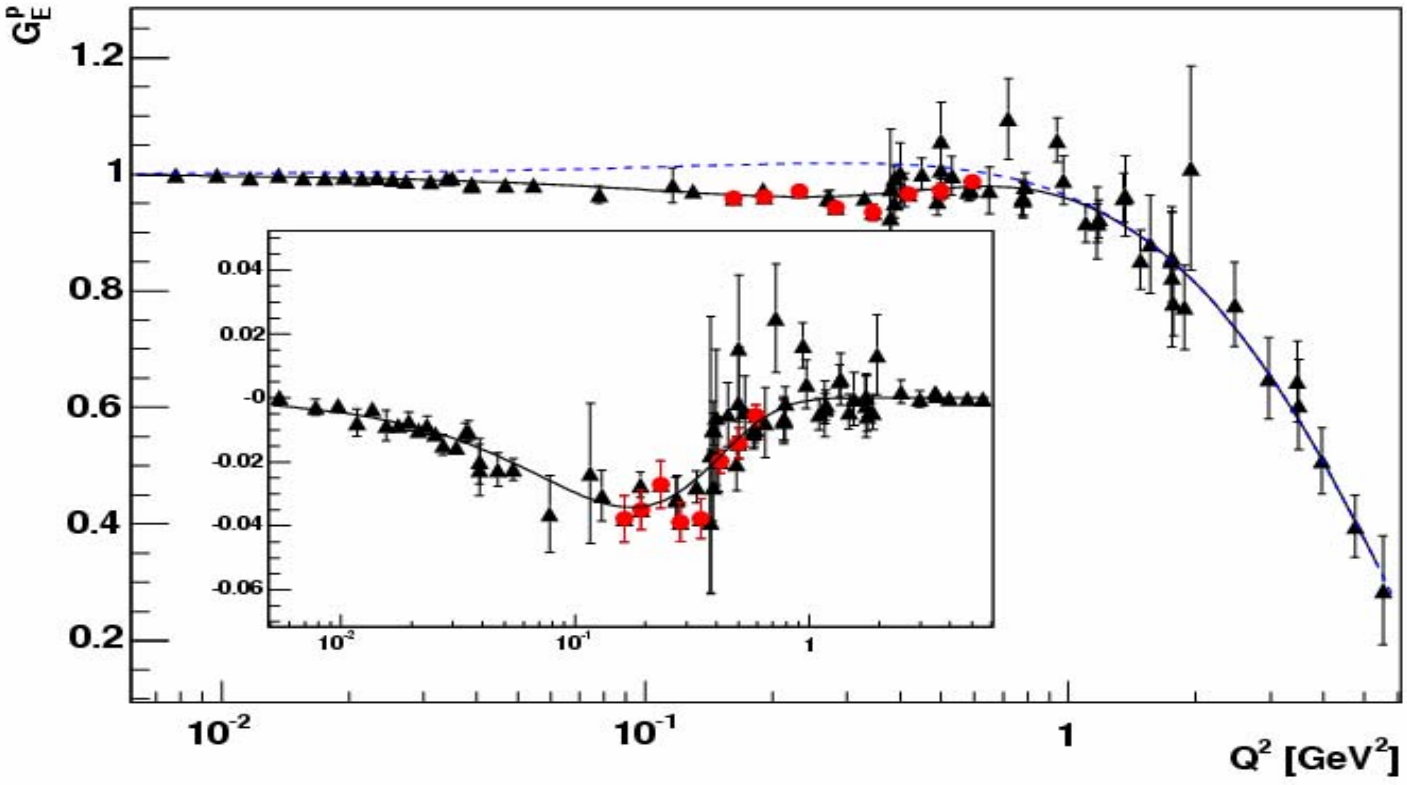

Preliminary BLAST G_M^p data

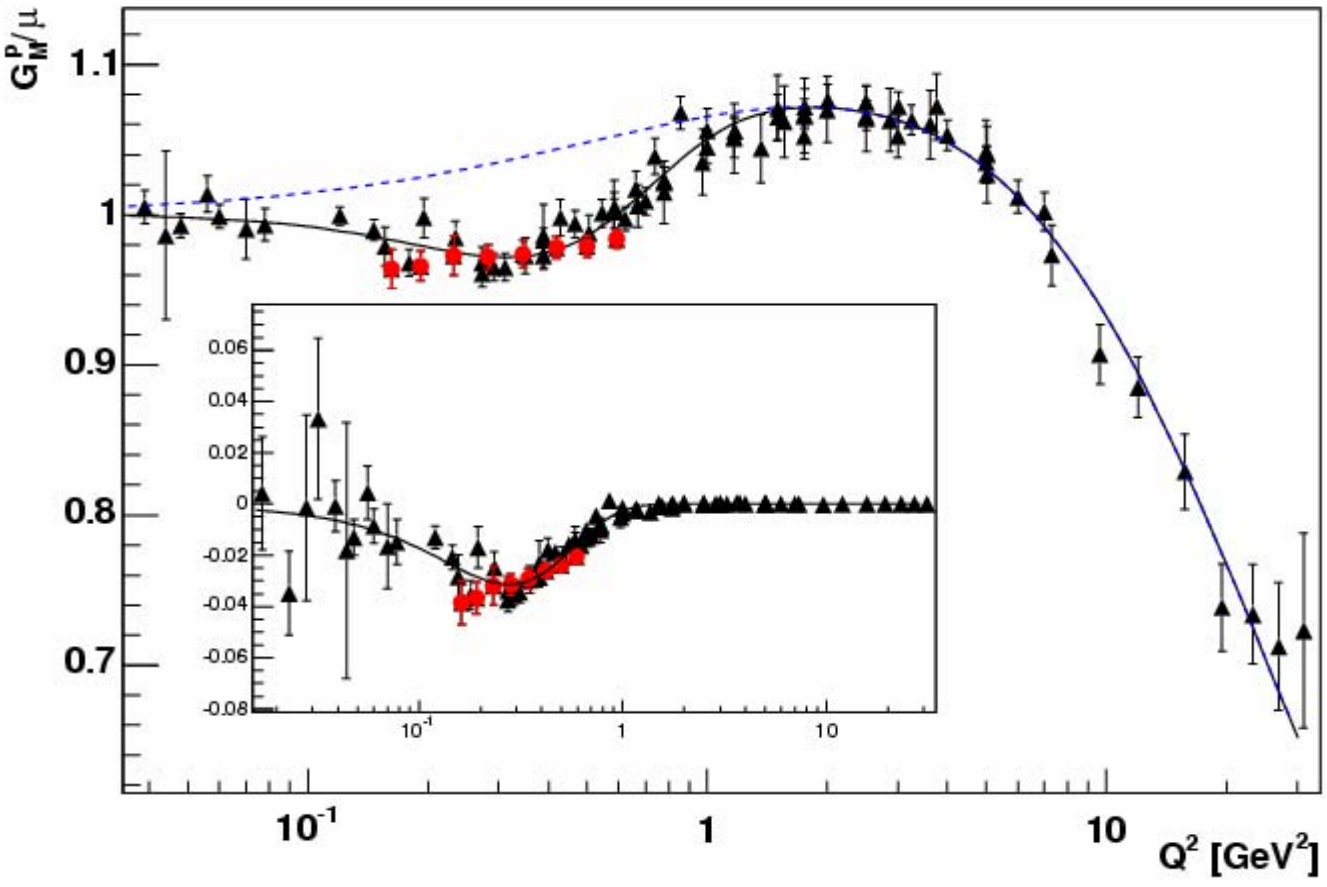

Preliminary BLAST G_M^n Data

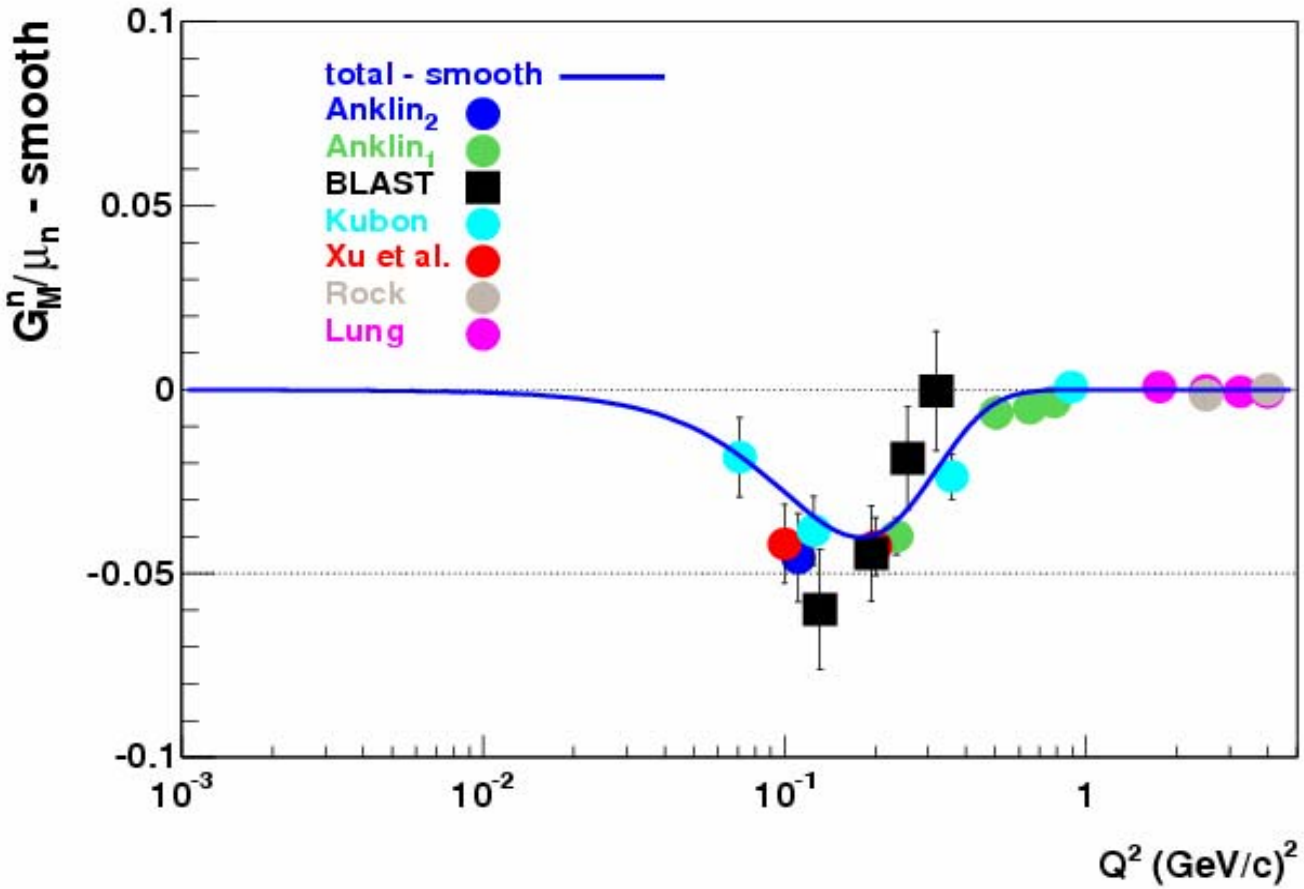

Preliminary BLAST G_n^E World Plot

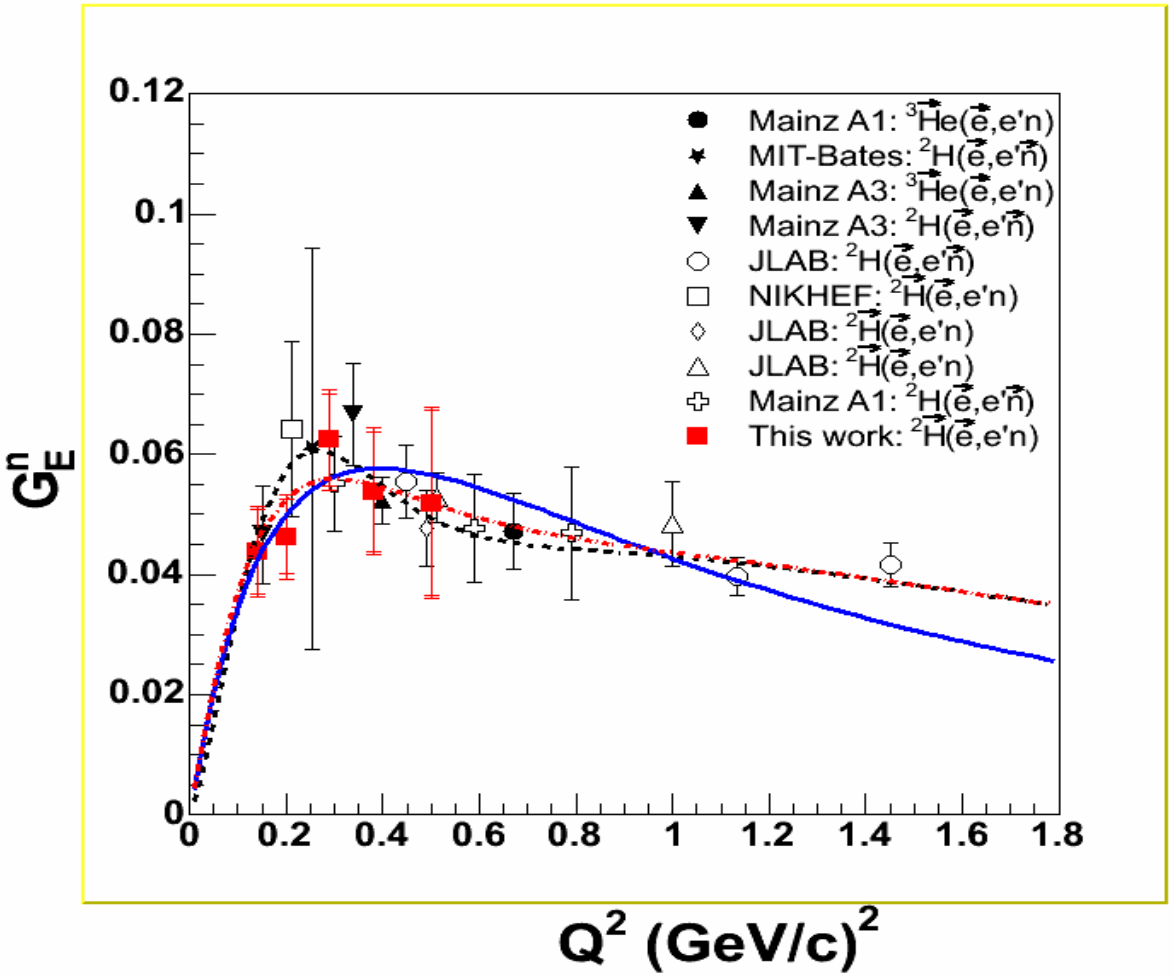

- Preliminary result
- Only 50% of data, final data should reach 0.5 (GeV/c)^2
- Use Arenhovel's calculations for G^n_M and contribution of G^n_E
- Need to combine with other BLAST measurements for global fit
- Provide low Q^2 data
  - Check bump
  - Pion cloud

BLAST Fit to World Polarization Data

- Remarkable consistency of all modern polarization experiments!

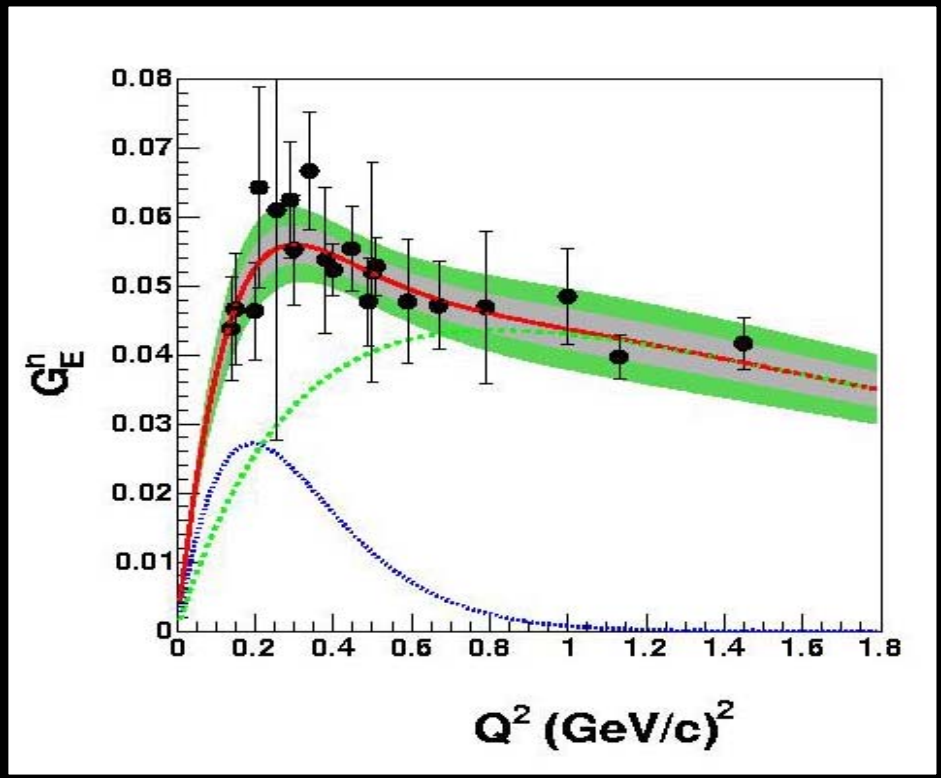

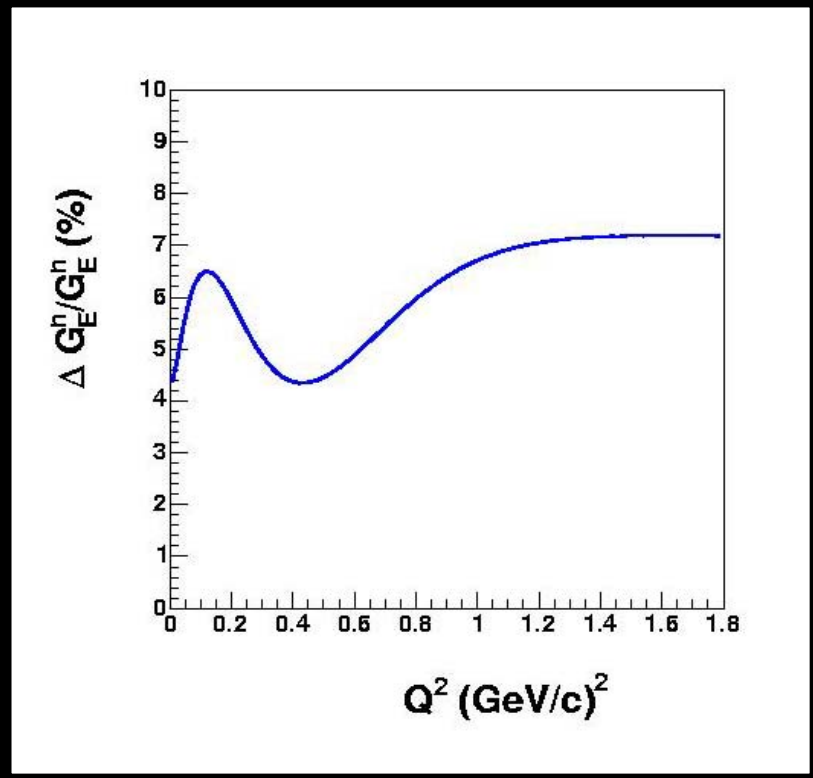

Global fit determines G_E^n to better than ±7%

"Density" from the BLAST Fit

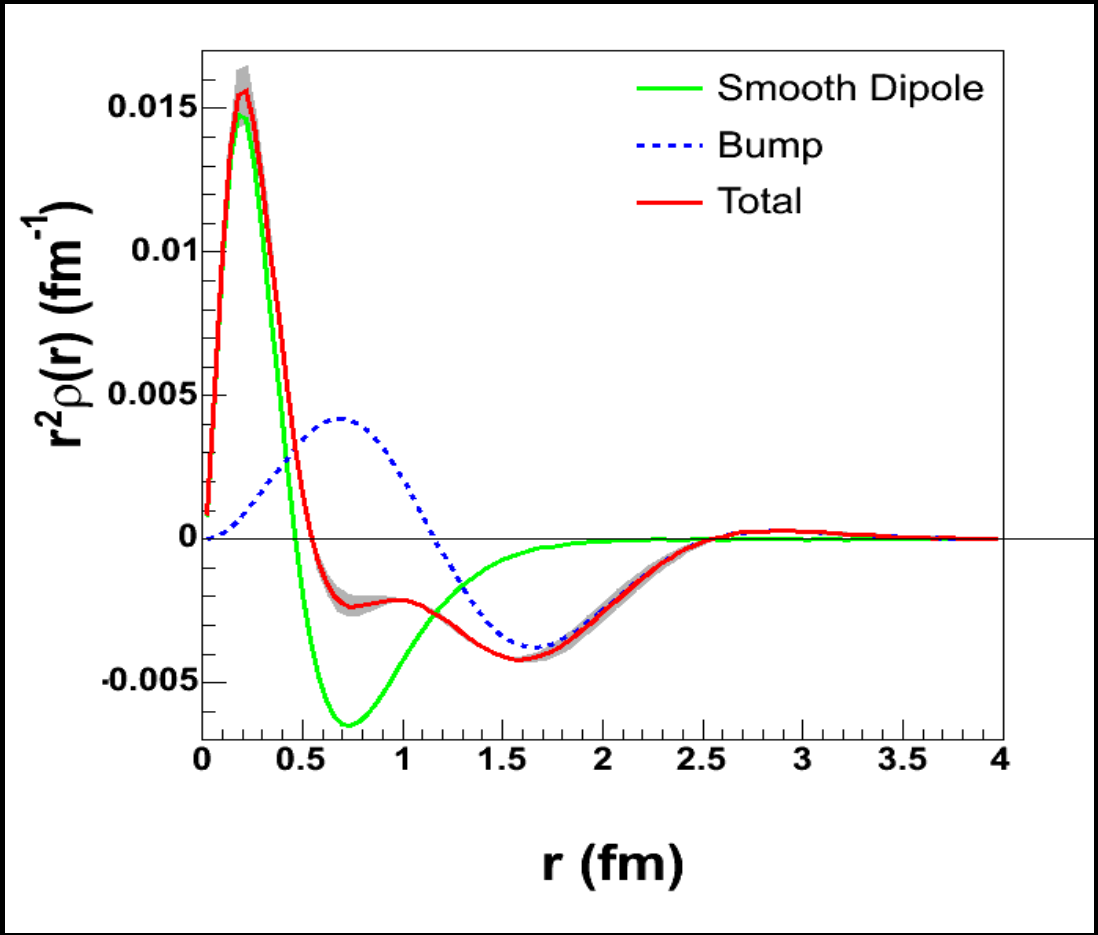

Non-relativistic Fourier transform of the neutron form factor

Smooth dipole corresponds to the constituent quark core

Bump corresponds to a diffuse pion cloud

were hampered by severe model-dependencies of the results, which therefore were uncertain to about 50%. The emerging results were describable by the so called Galster parameterisation, which started out from the usual dipole fit, which reproduced G_{E_p}, G_{M_p}, and G_{M_n} reasonably well and which was multiplied by some appropriate function in order to account for the condition $G_{E_n}(Q^2 = 0) = 0$ required by the vanishing charge of the neutron. This Galster form is given by

$$G_{E_n}(Q^2) = \frac{a_G\,\tau}{(1 + b_G\,\tau)} \cdot \frac{1}{(1 + Q^2/m_D^2)^2}\,, \qquad (1)$$

where $\tau = Q^2/(2m_n)^2$ and $m_n = 0.939$ GeV/c^2 is the neutron mass. The parameter m_D^2 was taken as the standard dipole value $m_D^2 = 0.71$ (GeV/c)^2 and $a_G = 1.73$ in order to reproduce the measured root mean square radius of the neutron of $\langle r^2 \rangle = -6\,dG_{E_n}(Q^2)/dQ^2|_{Q^2=0} = -0.115$ fm^2 as determined from the scattering of thermal neutrons [15]. Thus the only parameter free to be fitted to the data was b_G, and it was determined to $b_G = 4.59$. The Galster form has no particular theoretical justification and may rather hide the essential physics.

The collected data for G_{E_n} determined recently from polarisation measurements are depicted in fig. 1. These 15 data points, which are not hampered by model assumptions, have been taken with 8 very different experimental setups, and the data points taken with the same setups were taken over periods separated by long time intervals. Also, the setups had very different systematic errors and corrections due to nuclear binding effects. Therefore, it is justified to consider the data as statistically independent. Since the corrections are less certain for the measurements on ^{3}He than for the loosely bound deuterium, the measurements on the two targets are distinguished in fig. 1 by markedly different symbols. It is not the aim of this paper, however, to discuss critically these experiments but just to take this data set seriously and to investigate its essential features.

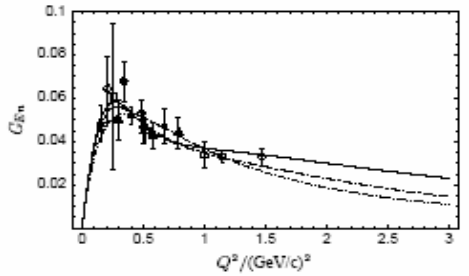

Fig. 1. The G_{E_n} data from polarisation measurements. The coding for reactions with the deuteron as a neutron target is: open square [1], filled diamonds [2,3], open diamond [4], open star [9], open triangle [14], open pentagon [12,13], and filled triangle [10,11], the measurements with ^{3}He are shown as filled squares [5–8]. The full curve depicts the fit of the parameters of eq. (2) to the data, the dashed dotted curve is a variant with slightly changed parameters as explained in the text, while the dotted curve is a fit using the Galster form, i.e. eq. (1).

It is evident from fig. 1 that the data can be as well regarded as a broad distribution and a peak around $Q^2 \approx 0.3$ (GeV/c)^2 not present in the smoother Galster fit.

In order to get some insight into the consequences of this alternative form we have added a term to the form of eq. (1) which is able to describe an additional peak with reasonable boundary conditions.

$$G_{E_n}(Q^2) = \frac{a\,Q^2}{(1 + b\,Q^2 + c\,Q^4)^5} + \\ + \frac{d\,Q^2}{(1 + e\,Q^2)(1 + f\,Q^2)^2}\,. \qquad (2)$$

The rms radius is now given by the sum of a and d, constrained to $(a + d)(2m_n)^2 = a_G = 1.73$, and we fixed a and d to $a = 0.37$ (GeV/c)$^{-2}$ and $d = 0.12$ (GeV/c)$^{-2}$. The parameters e and f were kept fixed at 0.5 (GeV/c)$^{-2}$. Minimising χ^2 yielded $b = 0.39$ (GeV/c)$^{-2}$ and $c = 1.68$ (GeV/c)$^{-4}$. Here we only want to have a parametrisation which reproduces the data within the experimental error bars without associating any particular physical meaning to the single parameters. In fact, as seen in fig. 1, this form reproduces the data well. It is not meaningful to go into any detail of an error analysis, instead we only show by the example of the dashed-dotted curve that with above parametrisation the "peak-region" and the tail to higher momentum transfers are essentially described independently from each other. For completeness we just mention that the χ^2 of the Galster form is by $\Delta\chi^2 = 4.8$ bigger than that of the two others.

As is well known [16], though sometimes questioned (for a discussion of this problem see ref. [17]), the Fourier transform of the electric and magnetic Sachs form factors $G_E(Q^2)$ and $G_M(Q^2)$ represent the charge and magnetic density distribution in the Breit frame, where the energy transfer $\omega = 0$ and the three-momentum transfer $|\mathbf{q}_{Breit}| = Q$; we denote these distributions by $\rho(r)$, which thus is given by

$$\rho(r) = \frac{4\pi}{(2\pi)^3} \int_0^\infty G(Q) \frac{sin(Qr)}{Qr} Q^2\,dQ\,. \qquad (3)$$

Refinements to this relation are discussed in detail in ref. [18] where it is also pointed out that corrections cannot be defined without model assumptions. Since we are interested in the gross features of the measured form factors and the spatial distributions, we base our further discussion on eq. (3). A more refined approach may result in some compression of the resulting distributions in r-space, which should not alter their salient features and which are therefore left out of consideration in this paper.

Fig. 2 shows the charge distribution in the neutron, ρ_{E_n}, calculated via eq. (3) with above given fits to G_{E_n}. We have plotted $r^2\rho_{E_n}(r)$ which represents the charge in a spherical shell at radius r. The charge distribution of the Galster fit shows the well known "aperiodic" shape with a positive bump in the interior and a negative bump at the outside of the neutron. This characteristic feature also results from an ansatz for the form factor with the superposition of two appropriate dipole forms, to which the Galster parameterisation is a good approximation.

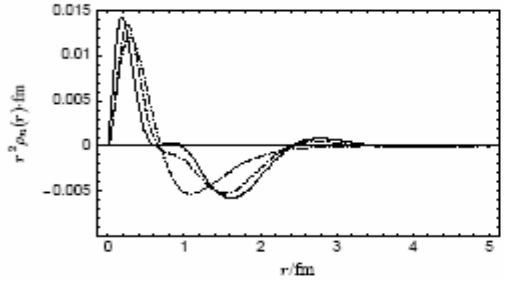

Fig. 2. The differential radial charge distribution of the neutron in the Breit frame as derived by a Fourier transform. The coding of the lines is that of fig. 1.

The fit with eq. (2), however, which accounts for the bump in G_{En} at $Q^2 \approx 0.3$ (GeV/c)^2, results in an oscillatory behaviour of $\rho_{En}(r)$ (see fig. 2). Though the oscillatory behaviour depends on the particular fitting form we shall show that it is the bump which shifts more charge to the outside than does the Galster fit. Since this outer region should be dominated by the pion cloud, the corresponding contribution should show up as a general feature also in the other form factors, where, however, a form factor bump of the same order of magnitude can only be expected to be a few-percent contribution.

With this in mind, we reconsider all four nucleon form factors in the following.

3 The data base

Table 1 gives an overview of the data which we have taken into consideration together with the Q^2-ranges which they cover.

For G_{Ep} we have omitted in the final analysis the data by Andivahis et al. [22]. In the Q^2-range of these data, $G_{Ep} \ll G_{Mp}$, thus its determination via a Rosenbluth separation is quite uncertain. In fact these data are clearly incompatible with the new results from polarisation measurements in which not the sum of $G_{Ep}^2 + \tau \cdot G_{Mp}^2$ is measured but the ratio G_{Ep}/G_{Mp}. It is straightforward to determine G_{Ep} from this ratio if one takes the prevailing G_{Mp} as known from measurement.

For G_{Mp} we took into account the same data as Kelly [18], i. e. the data by Hoehler et al. [29] up to $Q^2 = 0.15$ (GeV/c)^2 and those revised and compiled recently by Brash et al. [45]. In addition we also used the data by Hanson et al. [23].

For G_{En} we have only taken into account the data from polarisation measurements. The measurement in [35,23] give only G_{En}^2, thus the sign of G_{En} remains undetermined, and the errors are so large that the data can essentially be regarded as upper limits only; we did not take them into account in the fits. Other determinations of G_{En} were very uncertain due to the model dependency of the extraction of G_{En} from the measured cross sections, and we did not take them into consideration.

For G_{Mn} the data by Markowitz et al. [39] and by Bruins et al. [40] were omitted in the analysis as was already done

Measurement	Q^2-range	reference
G_{Ep}		
$p(e,e')$	0.01 - 0.05	Simon et al. [19]
	0.04 - 1.75	Price et al. [20]
	0.39 - 1.95	Berger et al. [21]
	(1.75 - 8.83)	Andivahis et al. [22]
$d(e,e'p)$	0.27 - 1.76	Hanson et al [23]
$p(\vec{e},e'\vec{p})$	0.37 - 0.44	Pospischil et al. [24]
	0.38 - 0.50	Milbrath et al. [25]
	0.40	Dieterich et al. [26]
	0.49 - 3.47	Jones et al. [27]
	3.50 - 5.54	Gayou et al. [28]
G_{Mp}		
$p(e,e')$	0.02 - 0.15	Hoehler et al. [29]
	0.16 - 0.86	Janssens et al. [30]
	0.39 - 1.75	Berger et al. [21]
	0.67 - 3.00	Bartel et al. [31]
	1.00 - 3.00	Walker et al. [32]
	1.50 - 3.75	Litt et al. [33]
	1.75 - 7.00	Andivahis et al. [22]
	2.86 - 31.2	Sill et al. [34]
$d(e,e'p)$	0.27 - 1.76	Hanson et al [23]
G_{En}		
$d(\vec{e},e'\vec{n})p$	0.15	Herberg et al. [3]
	0.26	Eden et al. [1]
	0.30, 0.58	Seimetz et al. [10]
	0.34	Ostrick et al. [2]
	0.49 - 1.47	Madey et al.[12,13]
	0.76	Glazier et al. [11]
	1.00	Day et al.[14]
$\vec{d}\,(\vec{e},e'n)p$	0.21	Passchier et al. [4]
	0.50	Zhu et al. [9]
$\overrightarrow{^3He}(\vec{e},e'n)$	0.40	Becker et al. [6–8]
	0.67	Rohe et al. [5,8]
$d(e,e')$	(0.27 - 1.76)	Hanson et al [23]
	(1.75 - 4.00)	Lung et al. [35]
G_{Mn}		
$d(e,e'n)p$	0.07 - 0.89	Kubon et al. [36]
	0.10 - 0.20	Xu et al. [37]
	0.11	Anklin et al. [38]
	(0.11 - 0.26)	Markowitz et al. [39]
	(0.13 - 0.61)	Bruins et al. [40]
	0.24 - 0.78	Anklin et al. [43]
$d(e,e'p)$	(0.27 - 1.76)	Hanson et al [23]
$d(e,e')$	1.75 - 4.00	Lung et al. [35]
	2.50 - 10.0	Rock et al. [44]

Table 1. Overview of data taken into consideration (Q^2 in (GeV/c)^2). The data left out in the final analysis are put into parentheses. The reactions are as indicated; $d(e,e')$ refers to quasi elastic scattering.

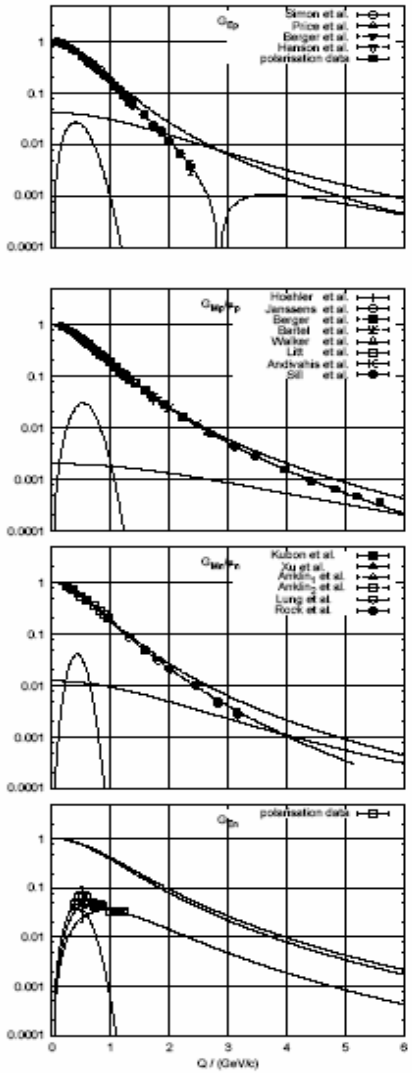

Fig. 3. The measured nucleon form factors and their description by the phenomenological fits. The full line represents the the sum of the two dipoles and the Gaussian, which are also shown separately, the second dipole form being multiplied by -1 in order to make it positive for this logarithmic plot. For G_{En} we also show the sum of the two dipoles separately.

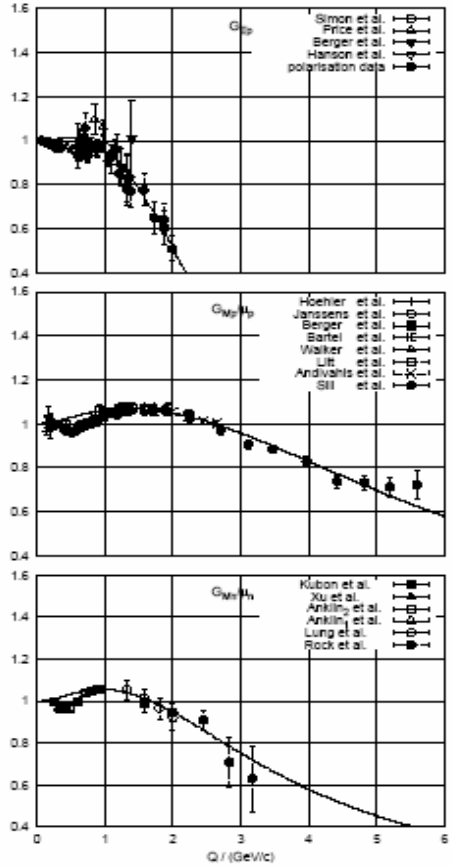

Fig. 4. The measured nucleon form factors and their phenomenological description divided by the standard dipole form factor. The full line represents the full fit, while the broken line is only the "smooth main part", i. e. the sum of the two dipoles.

This quantity is shown in fig. 7. Here, the contribution from the bump in the form factor is clearly visible as oscillation (net charge = 0). Its phase in r-space is such that it puts additional strength on the dipole form in the outer region with maxima between 1.5 (G_{M_P}) and 2.0 fm (G_{E_P}, G_{M_n}). The second dipole gives small and tiny contributions in the interior of $\rho(G_{E_P})$ and $\rho(G_{M_n})$, respectively, and is not visible in $\rho(G_{M_P})$. For G_{E_n} the oscillation gives the total $\rho(r)$ in the outer region centred around 1.7 fm, while the inner part is dominated by the dif-

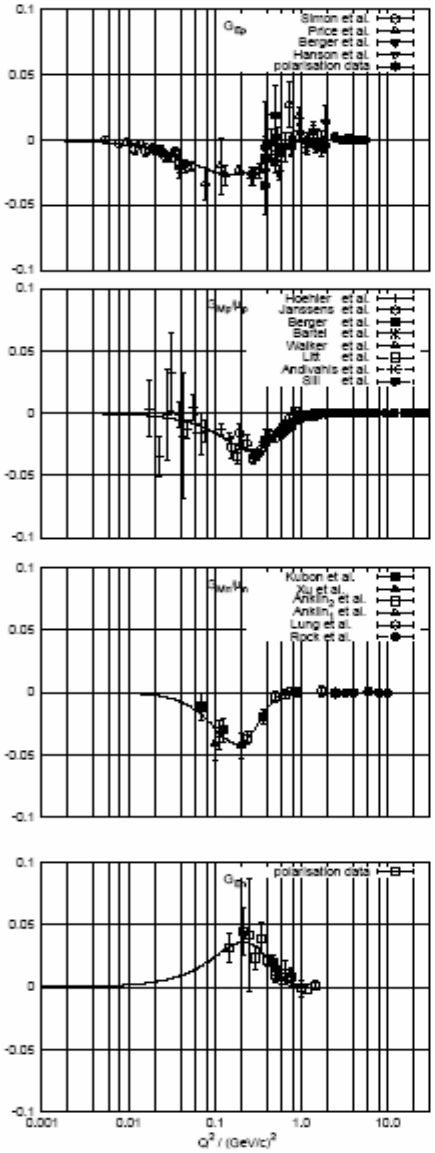

Fig. 5. The difference between measured nucleon form factors and the smooth part of the phenomenological ansatz with logarithmic x-scale for $Q^2/(\mathrm{GeV/c})^2$.

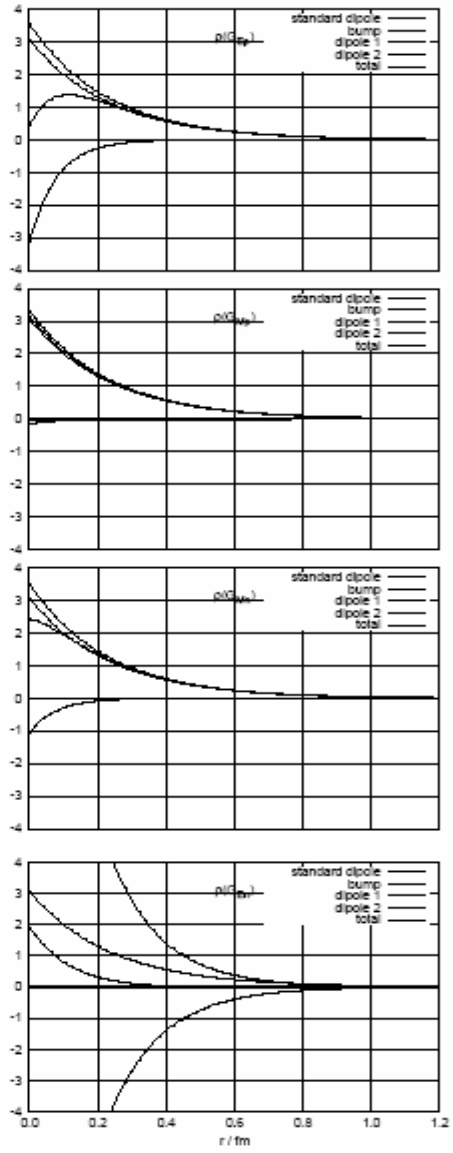

Fig. 6. $\rho(r)$ of the nucleons in the Breit frame. The units of $\rho(r)$ are fm^{-3}. The distributions are normalised to 1 for G_E^d and to 0 for G_{En}.

Chiral Dynamics of Baryons in a Lorentz Covariant Quark Model

Amand Faessler, Th. Gutsche, V. E. Lyubovitskij, K. Pumsa-ard

Institut für Theoretische Physik, Universität Tübingen, Auf der Morgenstelle 14,D-72076 Tübingen, Germany

(Dated: April 12, 2006)

We develop a manifestly Lorentz covariant chiral quark model for the study of baryons as bound states of constituent quarks dressed by a cloud of pseudoscalar mesons. The approach is based on a non-linear chirally symmetric Lagrangian, which involves effective degrees of freedom - constituent quarks and the chiral (pseudoscalar meson) fields. In a first step, this Lagrangian can be used to perform a dressing of the constituent quarks by a cloud of light pseudoscalar mesons and other heavy states using the calculational technique of infrared dimensional regularization of loop diagrams. We calculate the dressed transition operators with a proper chiral expansion which are relevant for the interaction of quarks with external fields in the presence of a virtual meson cloud. In a second step, these dressed operators are used to calculate baryon matrix elements. Applications are worked out for the masses of the baryon octet, the meson-nucleon sigma terms, the magnetic moments of the baryon octet, the nucleon charge radii, the strong vector meson-nucleon couplings and the full momentum dependence of the electromagnetic form factors of the nucleon.

PACS numbers: 12.39.Fe, 12.39.Ki, 13.40.Gp, 14.20.Dh, 14.20.Jn
Keywords: chiral symmetry, effective Lagrangian, relativistic quark model, nucleon electromagnetic form factors, meson-nucleon sigma-terms, strong vector meson-nucleon couplings

- Use bag model (constituent quarks)
- Restore chiral symmetry by requiring continuity of axial vector current across bag boundary
- Requires external pseudoscalar field (pion cloud)
- Couples pion cloud properties to const. quarks inside bag
- In F – W analysis, cloud fit to data

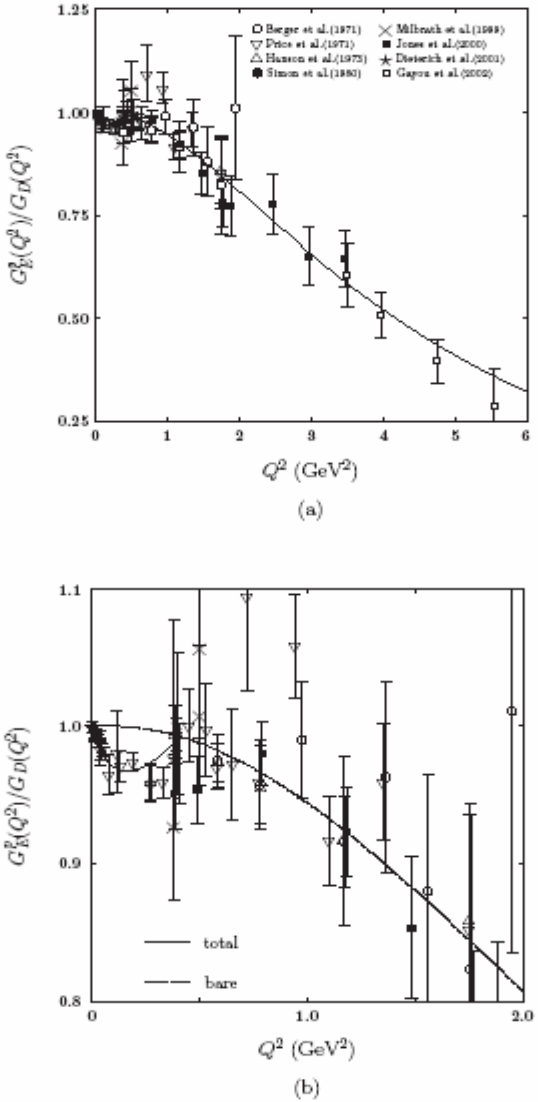

Fig. 5. *Ratio $G_E^p(Q^2)/G_D(Q^2)$: (a) Overall range, (b) Up to $Q^2 = 2$ GeV^2, the solid line is the total contribution and the dotted line is the bare contribution. Experimental data are taken from Refs. [58, 59, 60, 61, 62, 63, 64, 65].*

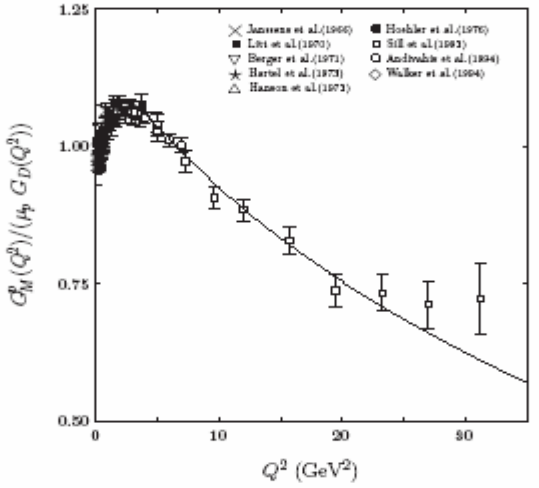

(a)

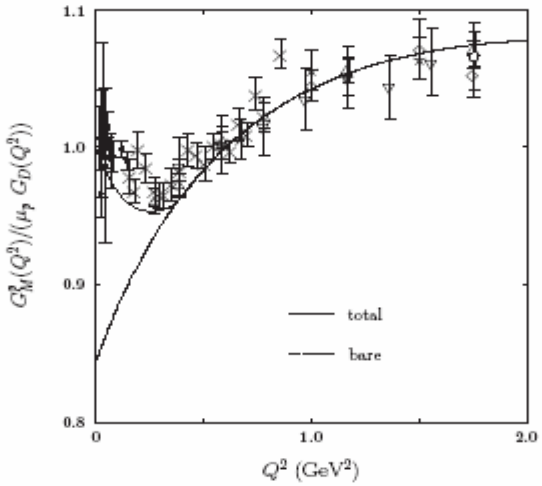

(b)

Fig. 6. *Ratio $G_M^p(Q^2)/(\mu_p G_D(Q^2))$: (a) Overall range, (b) Up to $Q^2 = 2$ GeV^2, the solid line is the total contribution and the dotted line is the bare contribution. Experimental data are taken from Refs. [60, 61, 66, 67, 68, 69, 70, 71, 72].*

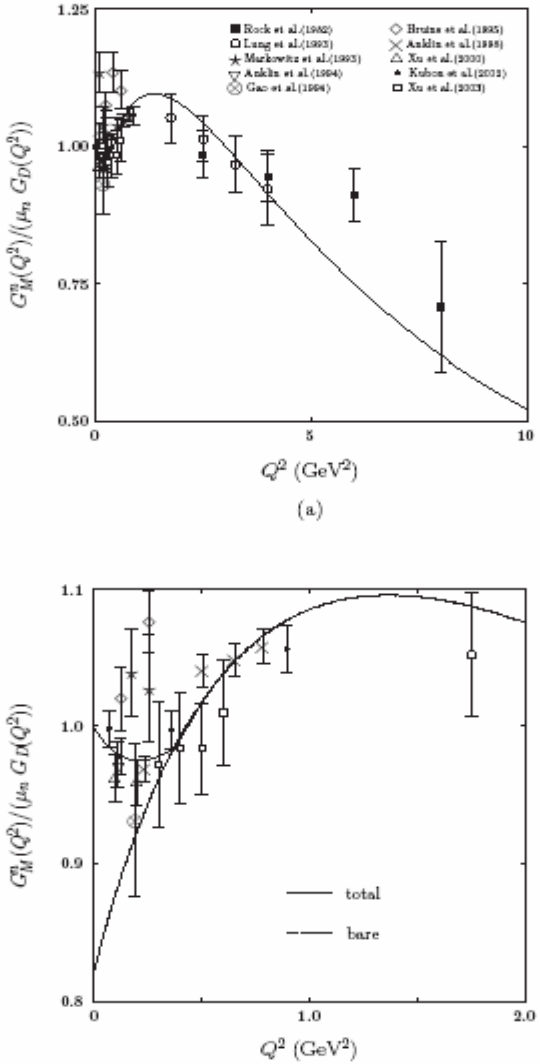

Fig. 7. *Ratio $G_M^n(Q^2)/(\mu_n G_D(Q^2))$: (a) Overall range, (b) Up to $Q^2 = 2$ GeV^2, the solid line is the total contribution and the dotted line is the bare contribution. Experimental data are taken from Refs. [73, 74, 75, 76, 77, 78, 79, 80, 81, 82].*

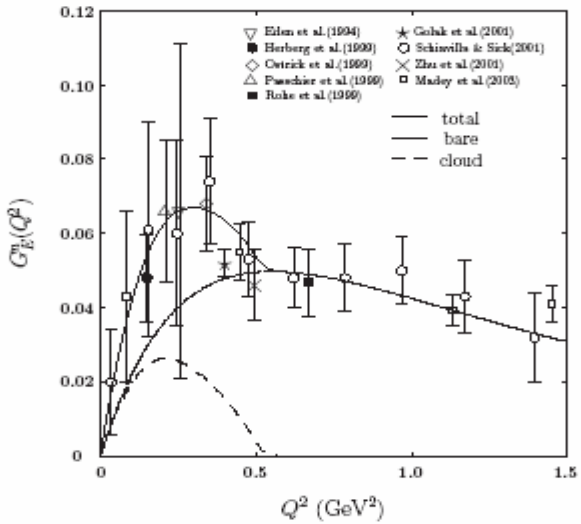

Fig. 8. *Neutron charge form factor $G_E^n(Q^2)$ and the contribution due to the meson cloud in comparison to the experimental data. Experimental data are taken from Refs. [83, 84, 85, 86, 87, 88, 89, 90, 91].*

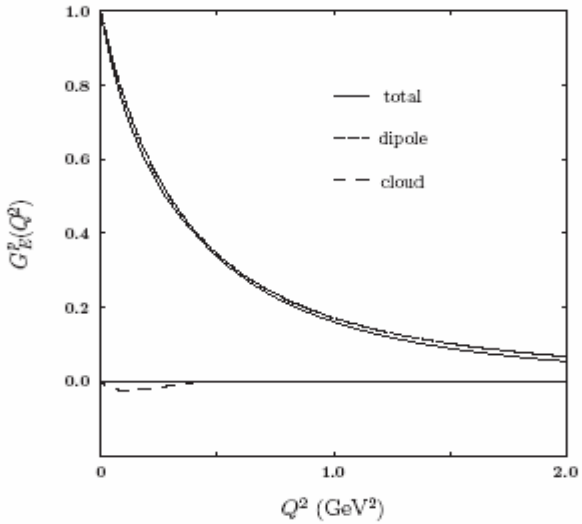

Fig. 9. *Proton charge form factor $G_E^p(Q^2)$ and the contribution due to the meson cloud in comparison to the dipole fit.*

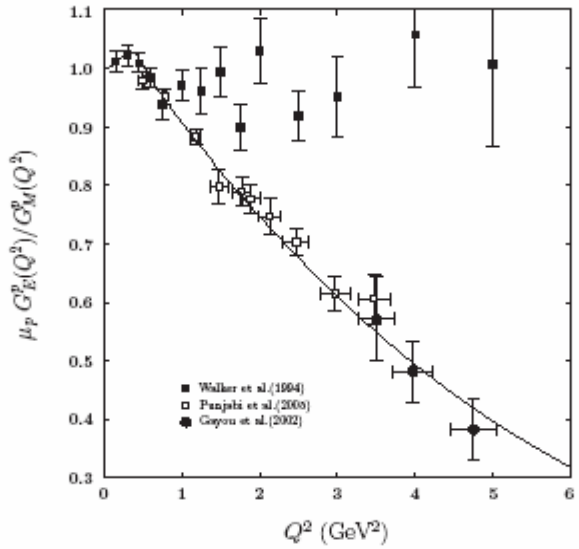

Fig. 16. *Ratio $\mu_p G_E^p(Q^2)/G_M^p(Q^2)$ in comparison to the experimental data. Experimental data are taken from Refs. [65, 69, 99].*

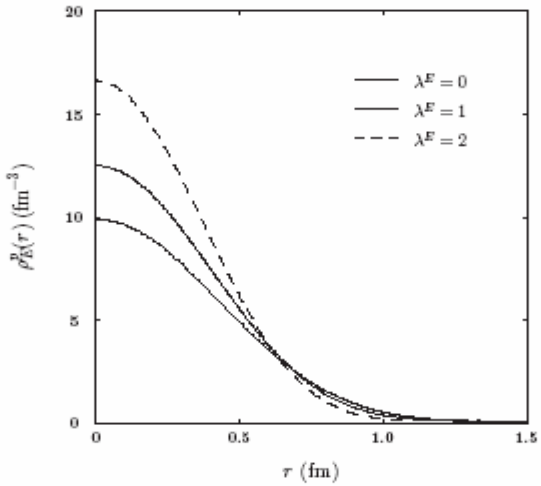

(a)

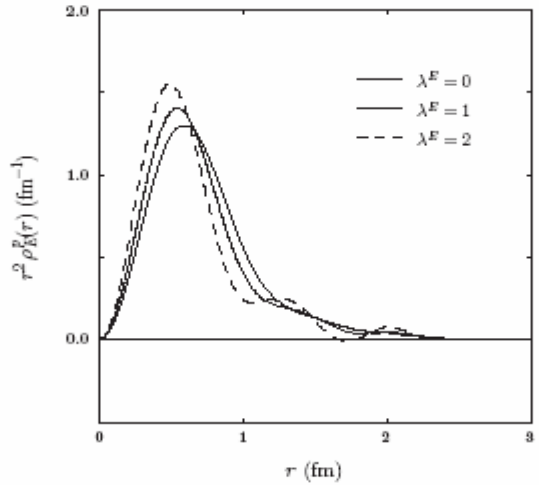

(b)

Fig. 17. *Variation of the charge density of the proton* $\rho^p_E(r)$ *and* $r^2\rho^p_E(r)$ *with* λ^E: $\lambda^E = 0$ *(solid line),* $\lambda^E = 1$ *(dotted line),* and $\lambda^E = 2$ (dashed line).

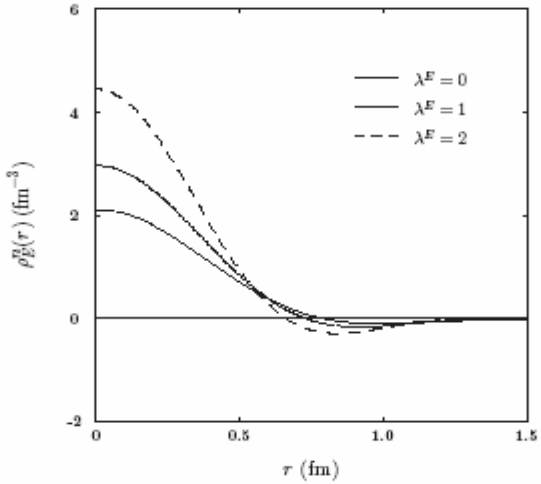

(a)

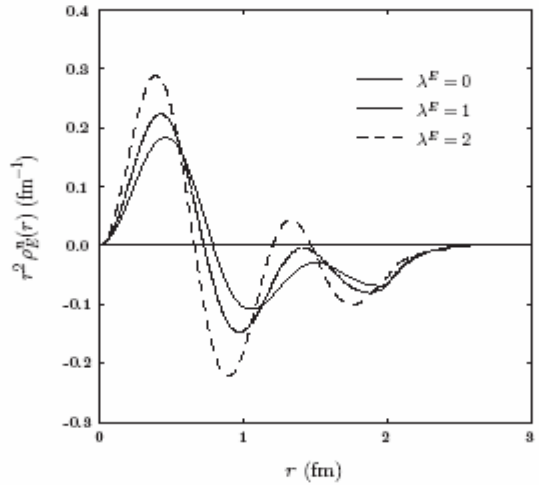

(b)

Fig. 18. *Variation of the charge density of the neutron* $\rho^n_E(r)$ *and* $r^2\,\rho^n_E(r)$ *with* λ^E*:* $\lambda^E = 0$ *(solid line),* $\lambda^E = 1$ *(dotted line),* and $\lambda^E = 2$ (dashed line).

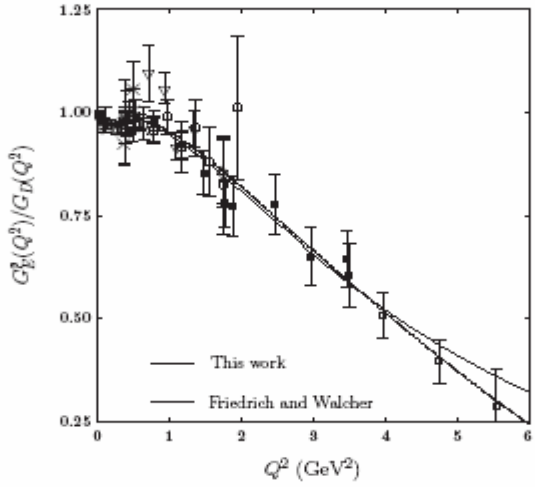

(a)

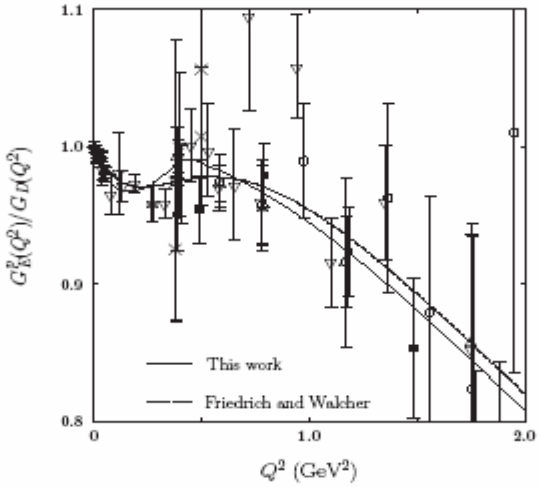

(b)

Fig. 21. *The ratio of the charge proton form factor to the dipole form factor, the comparison of our result (solid line) to the result reported in Ref. [55] (dotted line) : (a) overall range, (b) Up to $Q^2 = 2$ GeV^2. Experimental data are taken from Refs. [58, 59, 60, 61, 62, 63, 64, 65].*

G_E^p/G_D *vs.* Q^2

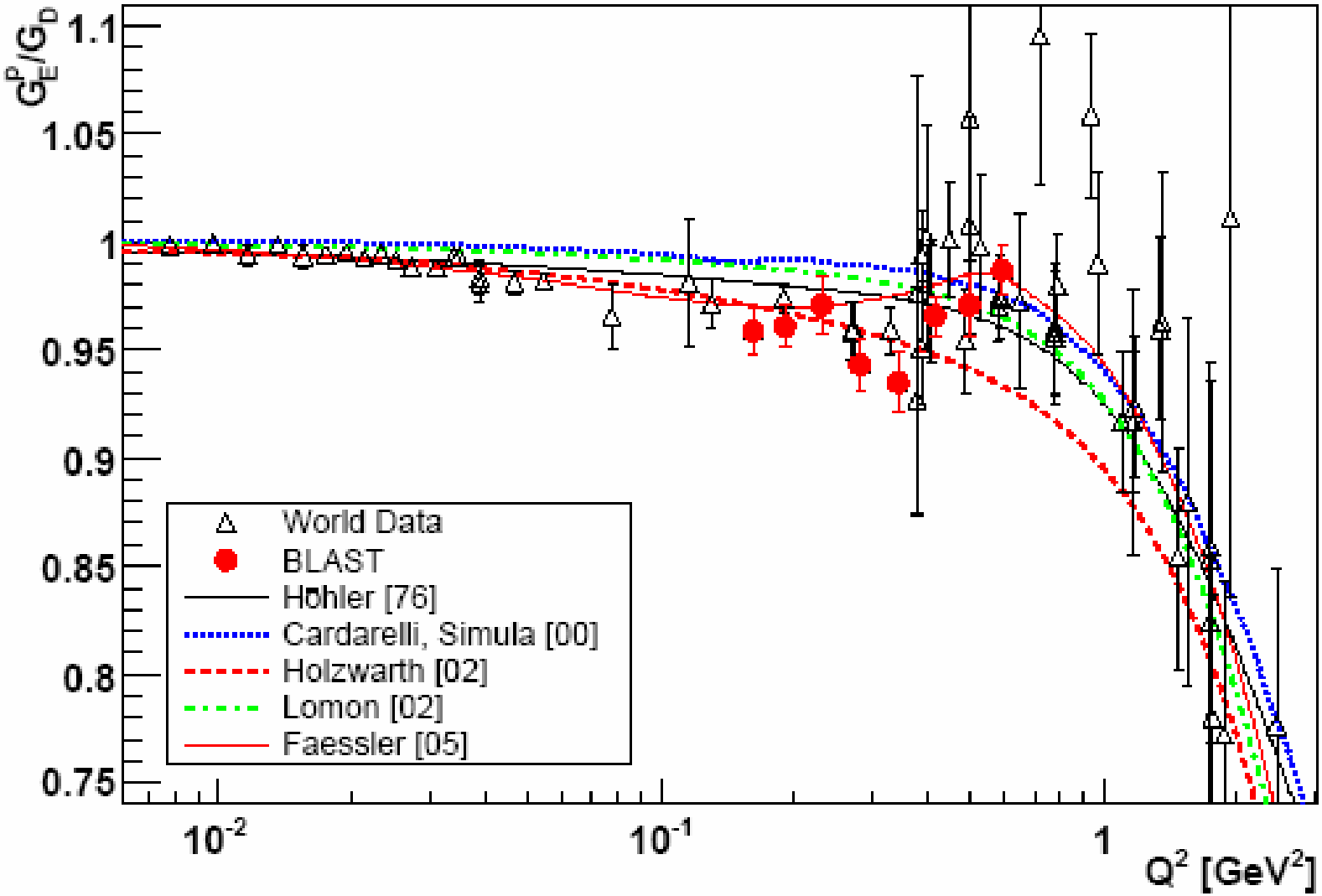
G_E^p/G_D
1.1
1.05
1
0.95
0.9
0.85
0.8
0.75
10^{-2}
10^{-1}
1
Q^2 [GeV^2]
World Data
BLAST
Höhler [76]
Cardarelli, Simula [00]
Holzwarth [02]
Lomon [02]
Faessler [05]

$G_M^p/\mu G_D$ *vs.* Q^2

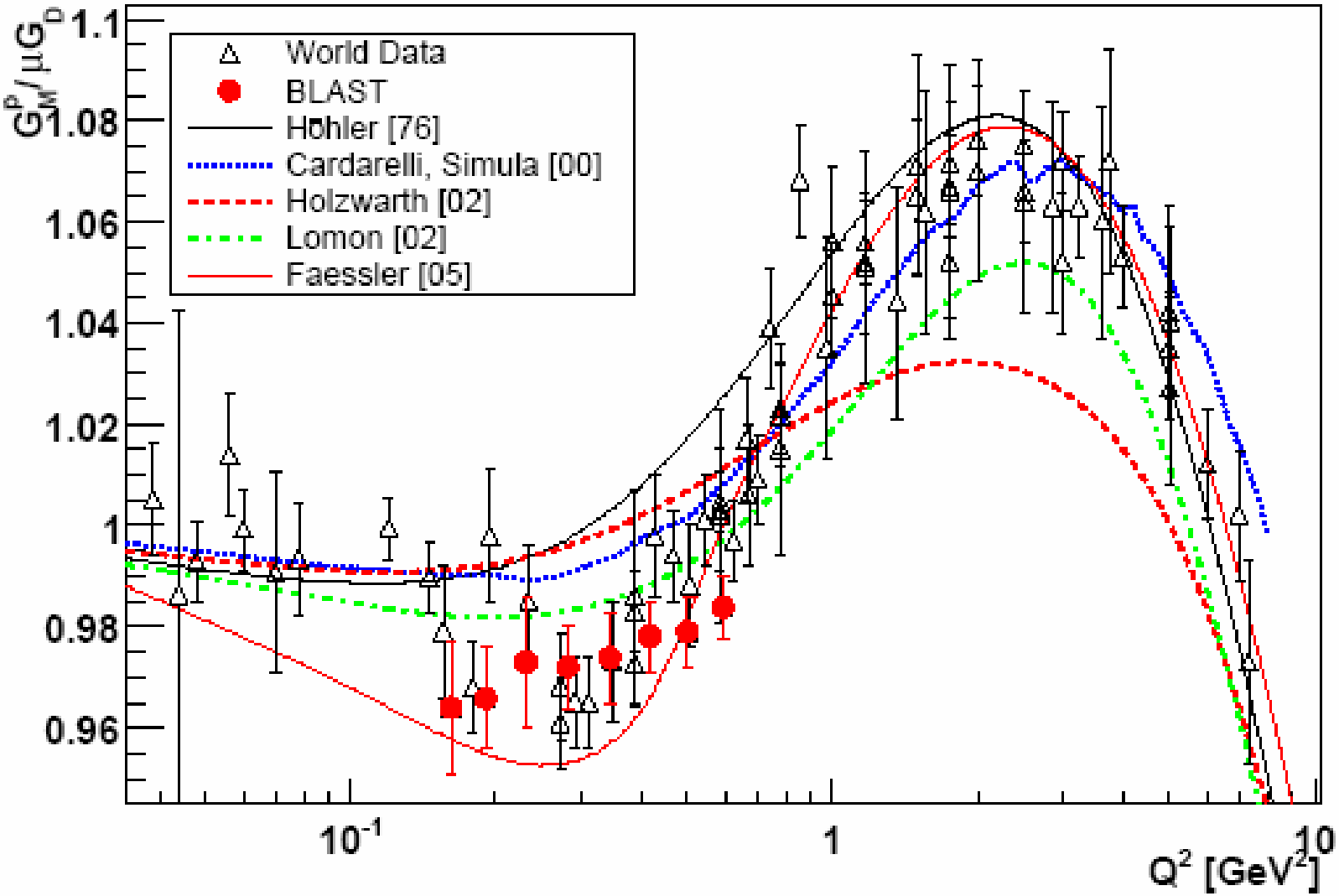

$\mu G_E^p/G_M^p$ *vs.* Q^2

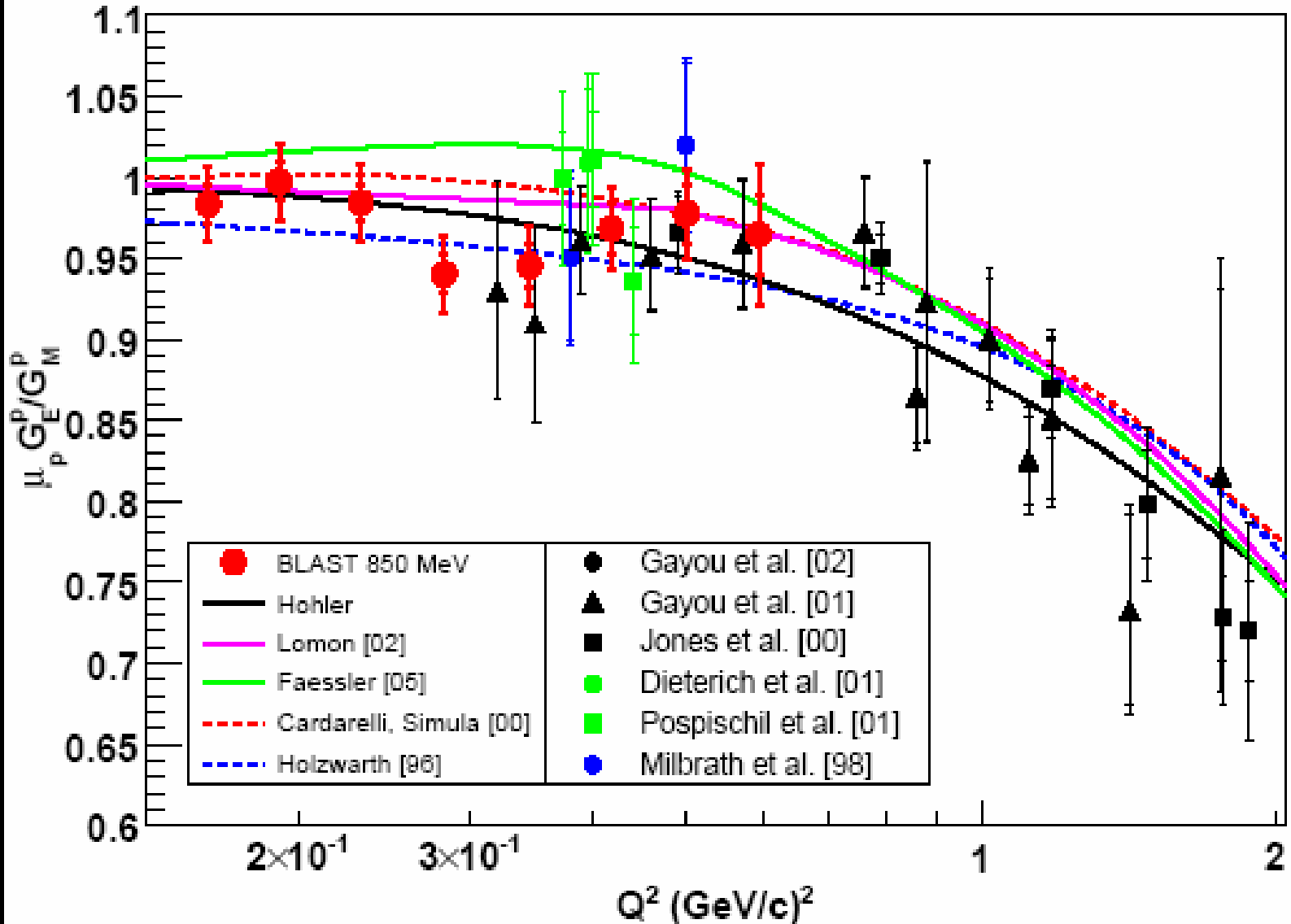

Summary

- 1st measurement of $\mu G_E^p/G_M^p$ using a polarized beam and a polarized target
- improvement in precision of $\mu G_E^p/G_M^p$ at $Q^2 = 0.1 – 0.5$ GeV^2
- Improved precision of G_E^n
- Sensitive to the pion cloud
- Self consistent description of all 4 form factors from the pion cloud